ESTIMATION OF REBAR CORROSION IN CONCRETE USING GROUND PENETRATING RADAR

By

RAKESH KRISHNARAJAPETE RAJU

Presented to the Faculty of the Graduate School of

The University of Texas at Arlington in Partial Fulfillment

Of the Requirements

For the Degree of

MASTER OF SCIENCE IN CIVIL ENGINEERING

THE UNIVERSITY OF TEXAS AT ARLINGTON

DECEMBER 2015

Acknowledgements

I would like to thank Dr. Nur Yazdani and Dr. Istiaque Hasan for all of their help they have given me during my time at UTA. Dr. Istiaque in particular has given me some very insightful ideas and guided as a mentor that have helped me to do this research successfully.

I want to thank Kshitij Kadam, Mohammad Bilal, Swapnil Dalvi, Joseph Williams, Surendar Kumar Gorrella and Giovanny Alzate for their help in carrying out the experiment.

Also, thanks to my wrestling family at UTA, whose support has always enabled me to keep moving forward.

Last but not the least, I want to thank everyone at UTA who I have been fortunate to become friends with over the past two years. It made the journey all the much more enjoyable.

December 3, 2015

Abstract

ESTIMATION OF REBAR CORROSION IN CONCRETE USING GROUND PENETRATING RADAR

Rakesh Krishnarajapete Raju, MS

The University of Texas at Arlington, 2015

Supervising Professor: NUR YADANI

The purpose of this research was to quantitatively relate the amount of rebar corrosion in concrete with the amplitude of electromagnetic waves generated from Ground penetrating radar (GPR). Many studies have been undertaken on qualitative measurement of corrosion, but there are very few studies regarding estimation of rebar corrosion quantitatively. This experiment involved the use of accelerated corrosion by impressed current technique to corrode the rebar inside the concrete and GPR to determine the extent of corrosion, while making a comparison with a stainless steel bar which was used as a cathode to create a galvanic cell action. Rebars were subjected to a constant 15 V power from a DC power supply while being immersed in a 5% NaCl till the corrosion products appeared on the concrete surface. Samples were removed from the tank after being subjected to their respective corrosion period and analyzed for corrosion extents and rebar mass loss. GPR readings were taken at the beginning,

after salt water immersion and at the end of their respective corrosion periods. The results indicated the unique value of amplitude of GPR electro- magnetic waves related to different extents of corrosion and rebar mass loss.

These results were later on compared with results obtained from a natural corrosion of # 4 (12.7 mm) rebar in bridge deck and percentage error was determined.

Table Of Contents

List of Illustrations

List of Tables

Chapter 1

Introduction

1.1 Background

Ground Penetrating Radar (GPR), also called as geo-radar or ground probing radar is a geo physical tool which is used in a wide range of applications. Over the past three decades, GPR has made contributions in the field of geology, infrastructure, forensics, military and security, agriculture, forestry, road inspection, geology, archaeology environment assessment transportation, public works and many more. This was possible because of its unique advantages, like being extremely accurate, fast, absence of drilling and digging, non-destructive, non-intrusive, easy to collect data, safe and digital media storage. GPR has also found its place in the field of RC structures where it is used to locate rebars, conduits, voids and cables in addition to imaging of reinforced concrete structures. This has made it one of the most versatile research tools that provides answers to many questions (Lai et.al 2011a).

One of the area which received great amount of attention in the field of RC structures was the determination of the amount of corrosion of rebar embedded in concrete. Various researches have done commendable studies in determining the extent of corrosion. Narayan et.al (1998), Hubbard et.al (2003) and Lai et.al (2010a, 2011a) studied the effect of steel corrosion on reflected waveform from the corroded bar. Their studies included the effect of accelerated

corrosion on some of the GPR parameters, like two way travel time, amplitude and frequency of reflected waveform. However, these findings reflected only on the evolution of rebar corrosion and failed to detect the amount of corrosion in the rebars. Correlation between parameters of GPR waveforms and steel corrosion extents was still not clear. Later on, researchers like Zhan et.al, Lai et.al (2012), and Hong et.al (2014) worked on correlating GPR waveform parameters with the progress of rebar corrosion. But these studies ended up relating them only qualitatively.

1.2 Objective

In this research, quantitative relationship between amount of corrosion of rebar in concrete and the maximum positive amplitude of GPR waveform is obtained. Effort was also made to highlight the effect of different phases of corrosion on parameters like two way travel time (TWTT) and dielectric constant of concrete cover with different rebar size located at different cover depths.

Specific objectives include:

- Study the effect of different phases of corrosion on maximum positive GPR amplitude.
- Study the variation of different rebar diameters with different cover depths on amplitude.

- Study the effect of different phases of corrosion on TWTT of reflected wave.
- Study the corrosion variation of different rebar diameters with different cover depths on TWTT.
- Study the effect of different levels of corrosion on dielectric constant of concrete cover.
- Quantitatively relate the percentage of mass loss of rebar due to corrosion with maximum positive GPR amplitude.
- Verification of experimental results obtained through accelerated corrosion with natural corrosion of a rebar in a bridge deck.

Chapter 2

Literature Review

2.1 Corrosion

2.1.1 Introduction

Corrosion is one of the natural phenomenon which is affecting the long term performance of reinforced concrete structures. Extent of corrosion has major impact on strength, deformational behavior, mode of failure, and ductility of RC structures. Therefore, it has become an important parameter in deciding the overall service life of the structure.

2.1.2 Corrosion mechanism

Overall corrosion process involves three mechanisms. They are as follows:

- Initiation stage
- De-passivation stage
- Propagation stage

In the initiation stage, de-passivation of the steel rebars takes place (Broomfield, 2002). As a matter of fact, rebars inside the concrete is protected against corrosion due to inherent alkalinity of the concrete, which forms an oxide protective layer called passive layer on the surface of the rebars.

However, due to the porous nature of concrete, this layer is damaged in the presence of chloride ions or carbon dioxide and the corrosion is initiated.

Second stage corresponds to development of corrosion products around the rebars in the presence of aggressive agents penetrated through the concrete cover. This can be referred to as the first stage of damage wherein the steel rebar dissolves to from iron oxides. The corrosion products thus formed spreads throughout the concrete pores and further induce micro cracking at the rebar and the concrete interface because of the tensile stresses generated by the expansive volume of the corrosion products.

In the propagation stage, the micro-cracks formed in the de-passivation stage starts expanding and extends toward the concrete cover. Eventually this leads to the spalling of the concrete which results in reduction in load carrying capacity of the RCC structures.

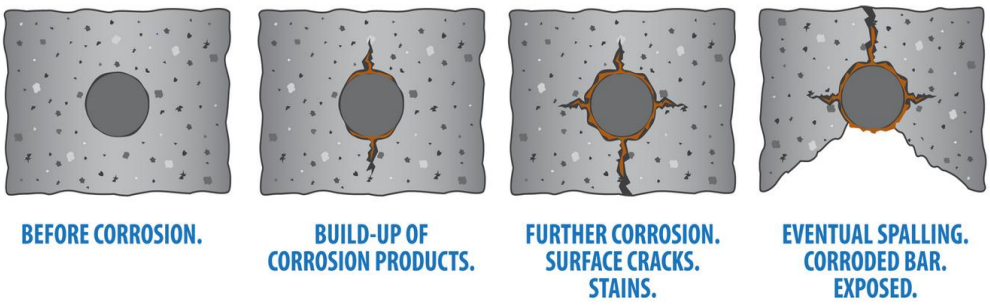

Figure 2-1: Different stages of corrosion mechanism (The Helpful Engineer, 2010)

2.1.3 Galvanic Corrosion

Galvanic corrosion occurs whenever two different metals of different electrode potentials comes in contact with each other in an electrolytic environment. Due to the electrode potential difference between the two metals one metal preferentially corrodes with respect to the other.

Generally, for galvanic corrosion occurs under the following conditions:

1. Electrochemically dissimilar metals
2. These metals must be in electrical contact
3. The metals must be exposed to an electrolyte

Out of two dissimilar metals one of the metals that is a nobler metal acts as cathode and the other metal acts as anode forming a galvanic couple in the presence of an electrolyte (Oldfield, 1998). Within the galvanic couple, anode i.e. the less noble metal corrodes with respect to the cathode at an accelerated rate. The level of accelerated corrosion depends on the difference in electrode potential between the two metals in contact. The higher the value of electrode potential, the greater will be the rate of corrosion of anode.

Therefore, utmost care is taken while selecting metals which are likely to come in contact with each other in such a way that the difference in electrode potential between the two is less. This will reduce the rate of corrosion. The knowledge of electrode potential of every metal can be obtained from a series

called galvanic series (Figure 2-2), which lists down the different metals/alloys in the order of their electrode potentials in flowing sea water.

Alloys/metals near the top of the galvanic series are considered less noble than the ones at the bottom.

The relative position of the alloys/metals in the series gives a good indication of which metals are more susceptible to corrosion. Lesser the distance between the metals in the galvanic series, slower will be the rate of corrosion. On the other hand, the farther the metals in the galvanic series the higher will be the risk of galvanic corrosion which should be avoided during the design.

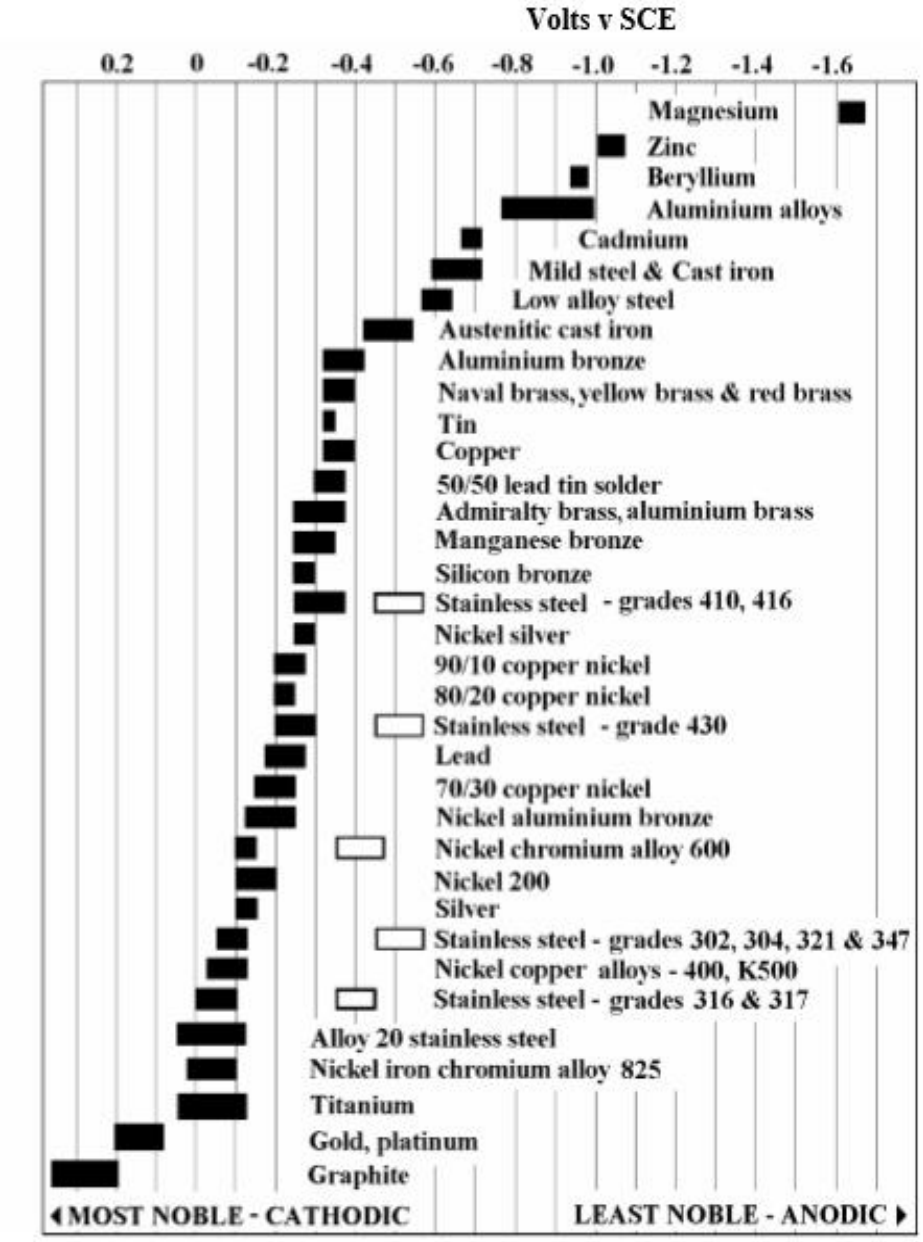

Figure 2-2: Galvanic series (Atlas tech note 7, 2010)

2.1.4 Factors affecting Galvanic Corrosion Mechanism

- The relative surface areas of cathode and anode in an electrolytic contact plays an important role in extent of corrosion (Mansfield, 1971). The surface area of cathode (nobler) metals has more influence on galvanic current responsible for corrosion. Small area of cathode in contact with the large area of anode would have minimal effect on overall corrosion rate of anode. On the other hand, large area of cathode in contact with the small area of anode would significantly corrode the less noble metal (anode). The larger the cathode, greater will be the oxygen reduction (or cathodic reaction) and hence greater will be the galvanic current.

    ⇨ This implies for accelerated corrosion, use Cathode rebar diameter higher than the anode rebar diameter which leads to large cathode area and a very small anode area, and for the exposed anodic area the corrosion rate will be correspondingly high.

    ⇨ Furthermore, small anode/cathode area ratio is undesirable as it would cause the galvanic current to concentrate onto small anodic area. This leads to rapid thickness loss of dissolving anode which should be avoided during the design.

- Painting of entire anode alone to decrease its area, would lead to intensified attack at breaks in the paint film.

- ⇨ For accelerated corrosion, avoid painting the cathode rebar and paint only the part of anode that is exposed to air thereby decreasing the area of anode relative to the cathode which increases the rate of corrosion at the anode.

- Choose metals that have dissimilar electro potentials. The more closely matched the individual potentials, the lesser the potential difference and hence the lesser the galvanic current (Oldfield, 1998).
  - ⇨ For accelerated corrosion, using different metals for the system is the easiest way of building up potential difference. Farther the metals in the galvanic series greater will be the potential difference and greater will be the galvanic current.
- Cathodic protection uses one or more sacrificial anodes made of a metal which is more active than the protected metal.
  - ⇨ For accelerated corrosion, use anodic metal whose corrosion reactivity is more than the cathodic metal. In other words use relatively less noble metals as anode.

2.2 Ground Penetrating Radar (GPR)

2.2.1 Introduction

Ground penetrating radar technique is a non-destructive testing (NDT) technique introduced in the field of reinforced concrete for the evaluation of its quality. It is a geophysical method that uses pulses generated from the radar to receive the information of the surface being surveyed. It has been widely used in engineering and environment surveys. GPR can be used to collect information about a variety of media, including freshwater, ice, soil, rock, structures and pavements.

The results obtained from GPR plays an important role in preservation and maintenance of concrete structures, especially in places where other techniques such as ultrasonic testing, infrared testing and pulse echo testing can't be used, GPR does a commendable job and serves the intended purpose with minimal labor and time needed. In general GPR technique can be used for various purposes, such as:

- Measurement of thickness of the road surfaces
- Study of geological formations in the field
- infrastructure
- Forensics
- Military and security

- Agriculture and forestry
- Road inspection
- Geology
- Archaeology
- Environment assessment
- Transportation
- Public works

In the field of RC structures, GPR is used to locate rebars, conduits, voids and cables in addition to imaging reinforced concrete structures.

2.2.2 GPR components and working mechanism

A GPR setup consists of three components. They are as follows:

1. Control unit
2. Antenna
3. Power supply

GPR equipment runs with a variety of the power supplies ranging from small rechargeable batteries to vehicle batteries depending on the conditions (Daniels, 2004).

The control unit contains the electronics that produces electromagnetic waves which the antenna uses for surveying. It also has a built-in computer with a hard disk and a memory which stores data.

The antenna consists of two components, a transmitter and a receiver. The transmitter sends the high frequency electromagnetic waves into the ground. Part of the signal is absorbed and the rest is reflected back to the receiver depending on the dielectric contrast between the two mediums. The lesser the dielectric value, the higher the speed of travel of signals. Dielectric constants of some of common the materials are listed in Table 2-1.

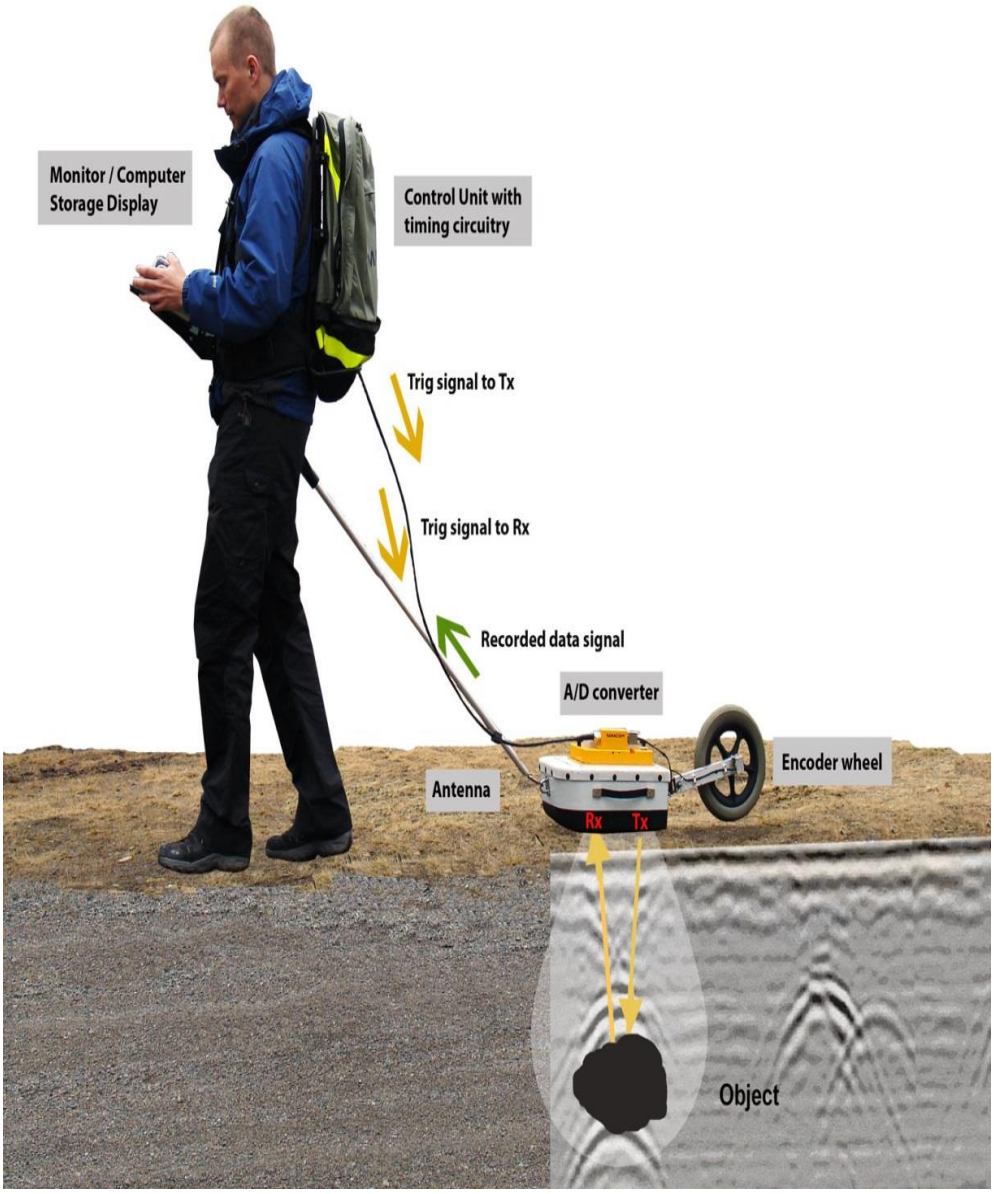

Figure 2-3: Various components of GPR (MALA Geoscience, 2014)

Table 2-1: Dielectric constants of common mediums

Media	Dielectric constant
Air	1
Snow	1-2
PVC	3
Asphalt	3-5
Ice	4
Concrete	4-11
Soil and Sediments	4- 30
Fresh and salt water	81

The reflected waves recorded by the GPR antenna contains information about time taken for its travel, also known as two way travel time (TWTT) and the amplitude of the signal. Amplitude defines the strength of the signal being reflected back.

GPR waves responds to changes in electrical properties which includes dielectric and conductivity of the material which are dependent on type of material and the moisture content. Higher conductivity and moisture content

makes the penetration of radar signals difficult. Also even a small dielectric difference of one can affect GPR data.

Another thing to note is that electromagnetic energy emitted by GPR may be affected in the presence of other electromagnetic devices (like cell phone, power supply unit, wires carrying electricity etc.), which may create noise and interfere making the data difficult to interpret. So it is advisable to collect the data keeping those devices away from the GPR.

In addition to the electrical properties, the depth of GPR data that can be obtained depends on the frequency of antenna used. Low frequency antenna gives information about deeper depths and larger targets, but with lower resolution, wherein higher frequency antenna gives information about shallower depths but offer a higher resolution images (Figure 2-4).

Depending on the application and depth range required appropriate, antenna frequencies are selected. Typical choice of antenna frequency can be made using Table 2-2.

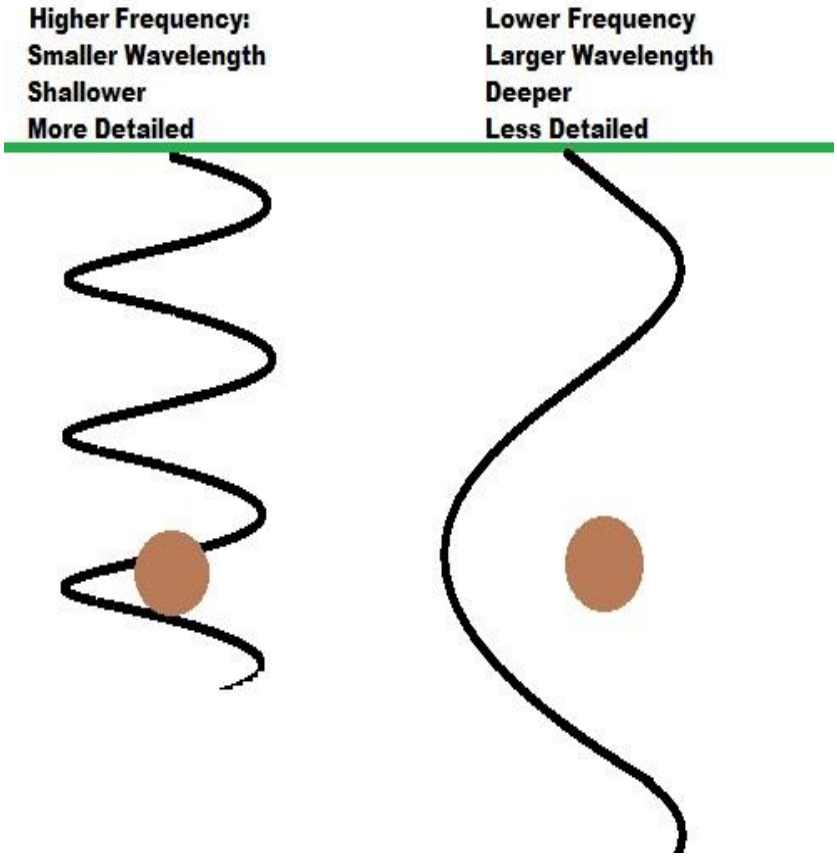

Figure 2-4: GPR antenna frequency (gprcourses.com, 2015)

Table 2-2: Various antenna frequencies and depth range (Geophysical Survey Systems, Inc. 2015)

Application	Primary antenna choice (MHz)	Secondary antenna choice (MHz)	Depth range (approx.), m (ft.)
Structural concrete, Roadways, Bridge Decks	2600	1600	0 - 0.3 (0-1)
Structural concrete, Roadways, Bridge Decks	1600	1000	0 - 0.45 (0 -1.5)
Structural concrete, Roadways, Bridge Decks	1000	900	0-0.6 (0- 2)
Concrete, Shallow soils, Archeology	900	400	0 - 1.0 (0 -3)
Shallow geology, Utilities, UST's, Archaeology	400	270	0 - 4.0 (0- 13)
Geology, Environmental utility, Archaeology	270	200	0 - 5.5 (0- 18.0)
Geology, Environmental utility, Archaeology	200	100	0 -9.0 (0- 30)
Geologic Profiling	100	MLF(16-80MHZ)	0 – 30 (0 -100)
Geologic Profiling	MLF (16-80)	None	> 30 (100)

2.2.3 GPR data output

When the GPR is moved along the surface of the target material, the antenna sends and receives electromagnetic waves that contains information about two way travel time and maximum amplitude of reflected wave. These reflections received by the receiver creates the picture of the surface resulting in a cross section, also known as a radar profile. The radar profile obtained in the detection of rebar within the concrete looks like a parabola. The tip of the parabola indicates the location of rebar. When this data is post processed using software application like RADAN (from GSSI), information such as two way travel time, maximum amplitude and frequency of reflected waves and dielectric constant of the medium can be extracted. Typical RADAN profile of the rebar within the concrete specimen is as shown in Figure 2-5.

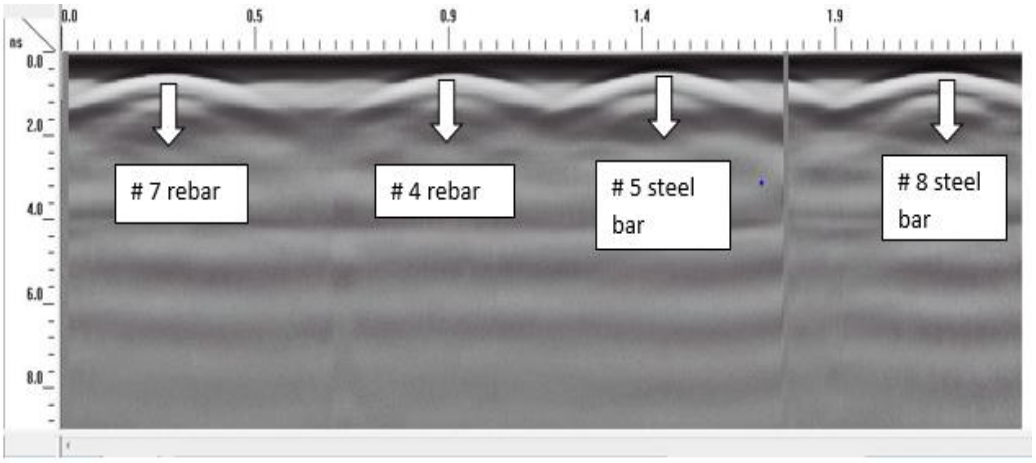

Figure 2-5: Parabolic profile of rebar obtained from RADAN

2.2.4 Advantages

As mentioned earlier GPR has various advantages over conventional equipment in the field of its application. They are as follows:

- Extremely accurate
- Fast
- Drilling and digging selected area is not required
- Non destructive
- Non-intrusive
- Easy to collect data
- Safe
- Digital media storage

2.3 Studies on concrete corrosion detection using GPR

Narayanan et.al (1998, 2003) analyzed reflected wave forms of GPR of corroded rebars to extract information on rebar state of corrosion and came up with a threshold level to differentiate between corroded and non-corroded bars.

Shaw (2003), developed neural network approach to estimate rebar diameter. Data were taken along both parallel and perpendicular directions using Multi-Layer Perception (MLP) neural network. It estimated rebar diameter effectively, but not accurately.

Hubbard et.al (2003) detected reinforcing bar corrosion using two nondestructive geophysical techniques which included GPR and electrical impedance. The study corroborated visual examination with destructive analysis of experimental block. He suggested that the GPR method provides quick and

high spatial resolution information of alterations at the interface of rebar and surrounding concrete. Radar amplitude had potential to detect rebar corrosion. On the other hand, electrical impedance technique provided valuable quantitative information about the corrosion process than the GPR which needed further study. This study concluded that the results obtained using GPR were largely qualitative and suggested that mechanistic or inverse models are yet to be developed to detect the changes in material properties due to corrosion.

Utsi (2004), used GPR along with numerical modelling to estimate rebar diameter using amplitude ratios of rebar signals along and across the electromagnetic field, which had accuracy of about 20%. He suggested that, as the ratio is easy to be distorted, practical application is highly dependent on the built environment of the experimental species. Failure to consider changes in dielectric constant of the concrete with increase in corrosion and lack of experimental data were considered as the two main drawbacks of this study.

Lai et.al (2012) performed a similar study on rebar corrosion using GPR at three different phases of corrosions. They are as follows:

- NaCl contamination phase, prior to NaCl and corrosion,
- De-passivation phase and,
- Corrosion phase

The maximum positive amplitude of reflected wave was found to change at different phases of corrosion. In the NaCl contamination stage, it was highest. In the second phase it decreased due to de-passivation of rebar and reduction in pH of the concrete. But with the increase in corrosion, amplitude started increasing with time which happens to be the third phase of corrosion.

A study conducted by Hong et.al (2014) also supported the fact that the peak to peak amplitude of direct and reflected waves will be maximum in the beginning, decreases during de-passivation stage and later on increases with increase in corrosion with time.

Chapter 3

Experimental procedure

3.1 Materials and equipment used

3.1.1 Rebars

As discussed earlier in order to simulate the galvanic corrosion in laboratory at an accelerated rate, two different types of steel bars were used. They are as follows:

- Mild steel rebars of grade 60 of sizes # 4 (12.7 mm) and #7 (22.22 mm)
- Type 304 stainless steel bars of sizes # 5 (15.87 mm) and # 8 (25.4 mm)

In order to study the variation of GPR parameter with different levels of corrosion, rebars of different diameters were chosen. Within the galvanic couple, mild steel bars acts as anode as they are relatively less noble than the stainless steel bars which acts as cathode. Due to the less nobility of rebars, corrosion occurs at the anode making it as a sacrificial metal during the accelerated corrosion process. Taking into account area ratio of anode and cathode (Mansfield, 1971), #4 (12.7 mm) rebar was coupled with #5 (15.87) steel bar and #7 (22.22 mm) rebar was coupled with # 8 (25.4 mm) steel bar.

Furthermore, rebars were pre-weighed before they were used as a reinforcement in the concrete specimen and weighed after the corrosion was stopped to determine the extent of corrosion in terms of rebar mass loss. Figure 3-1 shows the different steel bars used in this study.

Figure 3-1: Different types of steel bars used in the study

3.1.2 GPR Equipment

In this study, a GSSI GPR of frequency 2.6 GHz is used (Figure 3-2) to relate the GPR parameters with mass loss of rebars of varying diameter and concrete cover.

Figure 3-2: GPR equipment (Hasan, 2015)

According to electromagnetic theory (Stratton, 2007), the orientation of the GPR antenna influences the response from the target. First, the antenna axis

could be parallel to the direction of scan and the second, the antenna axis perpendicular to the direction of the scan (Figure 3-3). For this study normal orientation was chosen as its results are reasonable and practically reliable (Lai et.al, 2011).

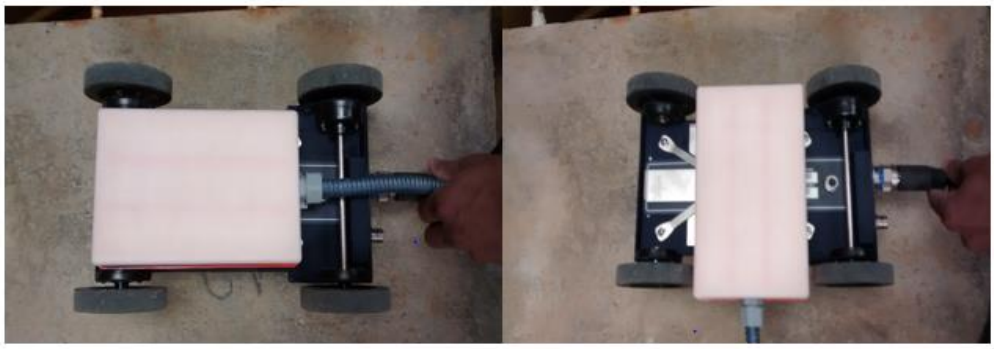

Figure 3-3: Orientation of GPR antenna

Initially various parameters related with GPR scan readings were adjusted in order to obtain high resolution data. They are as shown in Table 3-1.

Table 3-1: Initial GPR configurations

Antenna frequency	2.6 GHz
Scans/unit	512
Units/mark	6.0
Scans/sec	325

3.1.3 Power Supply and Circuit Configuration

In order to carry out accelerated corrosion by impressed current technique, a Vellemans DC power supply was used. It had a maximum capacity of 15 V and 3

amp. In this experiment a constant voltage of 15 volts was supplied to all the specimens. It was shown previously (Goucher, 2013) that this constant voltage was high enough to carry out accelerated corrosion within a small duration of time.

Figure 3-4: Power supply

In order to keep the supply of current continuous throughout the experiment, all the specimens were connected in a parallel combination so that the failure of one specimen would not affect the supply of current to the other specimens.

3.1.4 Salt solution

In the first stage of accelerated corrosion, the specimens were immersed in 5% NaCl solution (higher than the concentration of salt in sea water i.e. 3.8%) for seven days. To prepare this solution, cooking salt was dissolved in tap water.

3.2 Preparation of specimens

All specimens were cast using normal weight concrete with a water cement ratio of 0.60 and a maximum aggregate size of ¾ in. (19 mm). The mix proportion included 17.8lb./ft^3 (285 kg/m^3) of ordinary ASTM Type I Portland cement, 10.62 lb. /ft^3 (170 kg/m^3) of water, 58.3 lb./ft^3 (933 kg/m^3) of well graded fine aggregate (river sand) and 58.3 lb./ft^3 (933 kg/m^3) of crushed stone coarse aggregates. The average 28- day compressive strength from three cylinders was 4.9 ksi (35MPa). The concrete block specimens were 30” (76.2 cm) long, 15” (38.1cm) wide, and 8” (20.32 cm) high. Two # 4 (12.7 mm) and # 7 (22.22 mm) rebars of 60 ksi yield strength were placed near the top surface of the blocks. Each rebar was paired with a #5 or #8 Type 304 stainless steel rebar that served as the cathode in the accelerated corrosion process. Separate specimens were prepared with rebar cover depth of 1” (2.54 cm) and 2” (5.08 cm), as shown in Figure 3-5a & 3.5b. The regular rebars acted as anodes and experienced the accelerated corrosion.

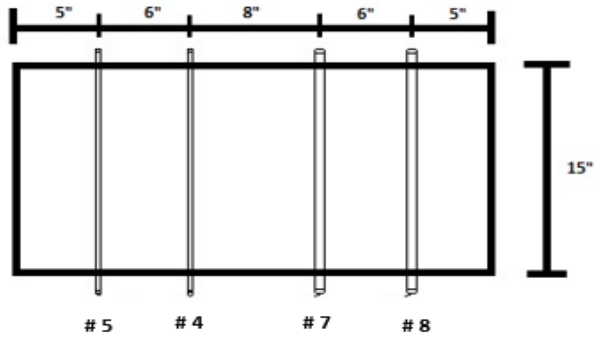

(a) Top view

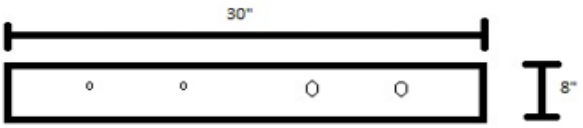

(b) Side view

(a) Specimen details

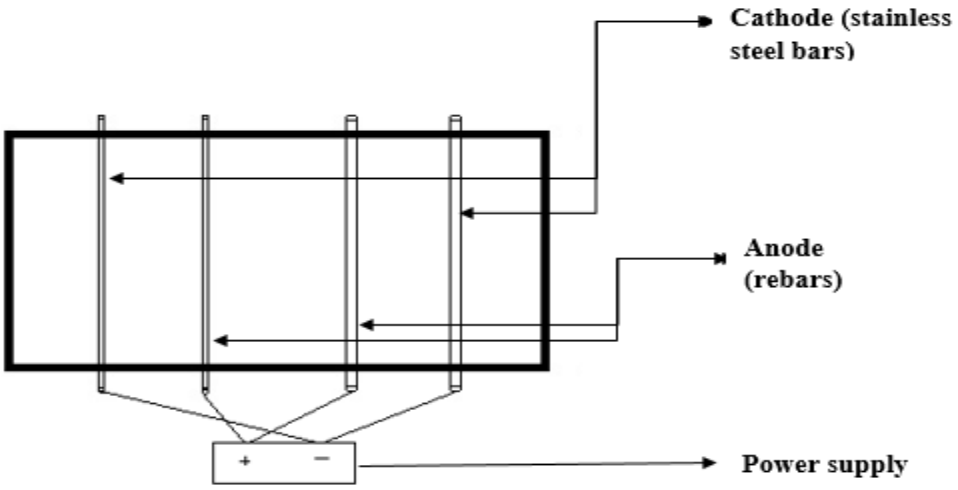

(b) Circuit connections

Figure 3-5 – Test setup

Construction of the specimens was undertaken in several stages. In the first stage, the wooden forms were oiled and the regular steel and stainless steel rebars were placed in proper positions in the plywood forms through pre-drilled holes The rebars extended out of the blocks to allow for the electrical connection required to impress the current (Figure 3-6). All specimens were cast horizontally, compacted, and trowel finished (Figure 3-7). After casting, the specimens were covered with polythene sheets for 24 hours and then de-molded. They were placed in a 100% humidity chamber for 28 days for curing (Figure 3-8).

Figure 3-6: Formwork and placement of rebars

Figure 3-7: Specimens after casting

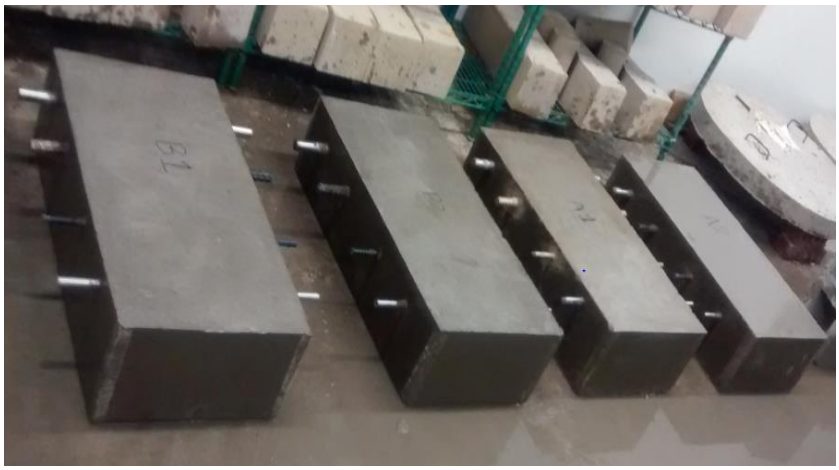

Figure 3-8: Curing of specimens in humidity chamber

3.3 Accelerated corrosion

3.3.1 Rebar protection

Before carrying out the accelerated corrosion, the ends of the projected rebars were painted with rust oleum and wrapped with Teflon tape (polymer) as shown in Figure 3-9. This was done to avoid corrosion of rebars outside the specimen that was meant for making electrical connections.

Figure 3-9: Wrapping of rebar ends with Teflon tape

3.3.2 Test Procedure

Accelerated corrosion on all six specimens was carried out in two stages. First, two specimens with 1 in. (25 mm) and 2 in. (50mm) cover (designated as A1 and A2 in Table 3-1, respectively) were subjected to extensive accelerated corrosion. In this study, this stage was designated as “maximum corrosion” and occurred at 30 days. Based on the time required for maximum corrosion, specimens B1 and B2 were subjected to accelerated corrosion for two third of the time taken for maximum corrosion (20 days). Specimens C1 and C2 were subjected to accelerated corrosion for one third the time taken for maximum corrosion (10 days). These stages were arbitrarily chosen to study the variation of GPR parameters with different extents of rebar corrosion in concrete.

A total of six specimens were prepared, for different concrete covers and different extents of corrosion.

Table 3-1: Experimental matrix

Accelerated Corrosion period (days)	Specimen designation	Concrete cover, in.(mm)
10	C1	1.0 (25)
	C2	2.0 (50)
20	B1	1.0 (25)
	B2	2.0 (50)
30 (maximum corrosion)	A1	1.0 (25)
	A2	2.0 (50)

3.3.3 GPR reading sequence

For initial GPR scanning, the specimens were placed in a tank. The tank container was coated with rust oleum in order to prevent its corrosion and the specimen top surface was scanned (Figure 3-10). Thereafter, each specimen was submerged in a water bath containing 5% salt (NaCl) solution (more than the 3.1–3.8 % salinity in seawater) for seven days (Figure 3-10). Saline water level was maintained at 1" (25 mm) above the specimens. This allowed the saline solution to ingress into the pores of the concrete and initiate the corrosion. After seven days, the water level was lowered to 1" (25 mm) below the rebar level. Two days of waiting period was needed to ascertain that the concrete surface was touch dry. This allowed surface current conductivity to be stable, so that surface water did not affect the GPR waveforms when the next current impression step was started. At this time, a second GPR scanning was performed. The last GPR scan was performed at the end of the 30 day maximum corrosion period.

Once the period required for maximum corrosion was determined, specimens C1, C2, B1 and B2 were simultaneously subjected to accelerated corrosion. A separate arrangement made of concrete block and PVC liner (waterproofing material) was made to accommodate all four specimens and the experiment was carried out as described for A1 and A2.

(a) Before immersion

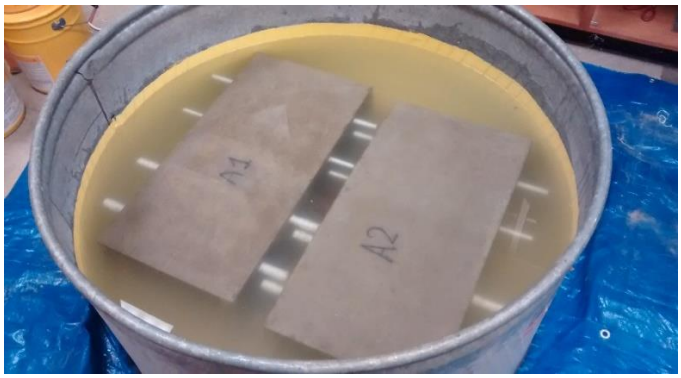

(b) After immersion

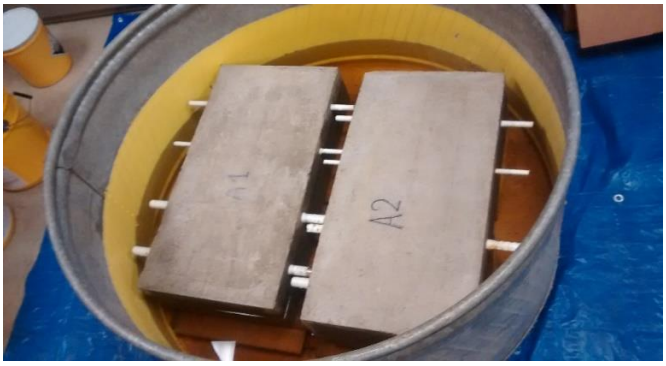

(c) After water level was lowered below rebar level

Figure 3-10: Different stages in initial GPR readings

(a) After immersion

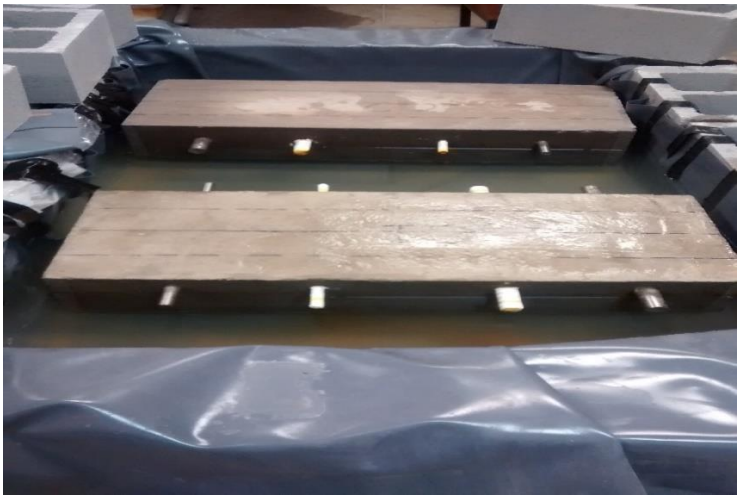

(b) When water level was lowered below rebar level

Figure 3-11: Arrangement for specimens C1, C2, B1 and B2 during accelerated corrosion

(a) Accelerated corrosion setup

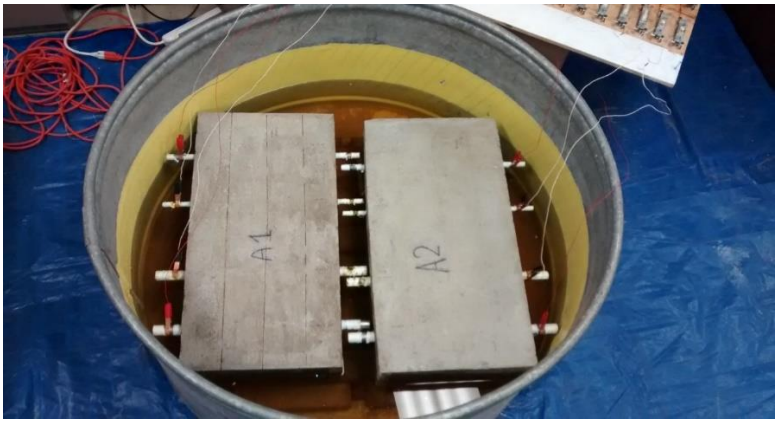

(b) Circuit connections for rebars

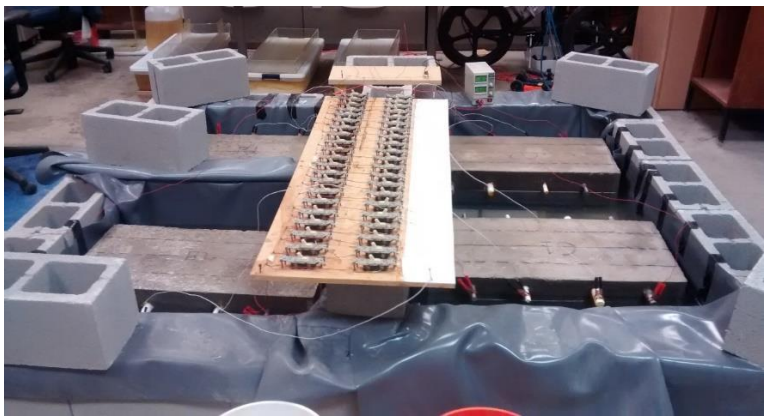

(c) Test setup for specimens C1, C2, B1 & B2

Figure 3-12: Test setup for impressed current technique

3.3.4 Impressed current technique

After the second GPR scan, the accelerated corrosion set up was hooked up with the rebars and the impressed current was applied. During the additional 30 day period, potential difference was monitored across the rebars every day to ensure constant voltage supply. The top surface of concrete was wetted by spraying water so that the corrosive environment was maintained. Any burnt out electrical connections (due to overheating) were replaced to ensure constant voltage supply. Specimens were checked for any cracking of concrete surface, deposition of corrosion products on concrete surface, and excessive localized current leading to pitting corrosion in the rebars projected outside the specimens.

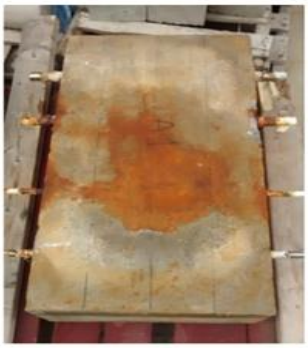

(a) Top view

(b) Side view

Figure 3-13 – Top and side view of specimen A1 at the end of 30 days

(a) Top view

(b) Side view

Figure 3-14 – Top and side view of specimen A2 at the end of 30 days

Accelerated corrosion in specimens A1 and A2 was performed first. By 30 day time, sample A1 had significant accumulation of corrosion products over the top surface and the experiment was stopped. Accelerated corrosion in sample A2 was ended when the significant pitting corrosion due to localized current at the rebar projections was observed on the 30th day.

At the end of corrosion period, specimens were cut open to find the extent and amount of rebar mass. Due to the complex nature of the corrosion various

measurements were made to define the behavior of concrete during corrosion process. One of the methods employed is explained in next few sections.

3.3.5 Current Measurements

Even though the applied voltage was kept constant at 15V, the current used to vary depending on the extent of penetration of salt solution through the pores of the concrete. In other words, it was dependent on the number of electrical paths created due to the development of micro-cracks as the salt solution flowed through the concrete layers and came in contact with the rebars. As the corrosion process continued, high current measurements was indicative of the increase in corrosion with the passage of time. At the rebar projections in concrete with 2" (50 mm) cover (A2), pitting was seen, excessive current was measured on 30^{th} day, which was indicative of the failure of the specimen. Once this occurred, passage of current was stopped and specimen was removed from the tank.

3.4 GPR measurements

In order to evaluate the uniformity of corrosion, GPR readings along three different locations on the specimen surface were taken, as shown in Figure 3-15. Along each line of consideration, three different GPR scans were performed.

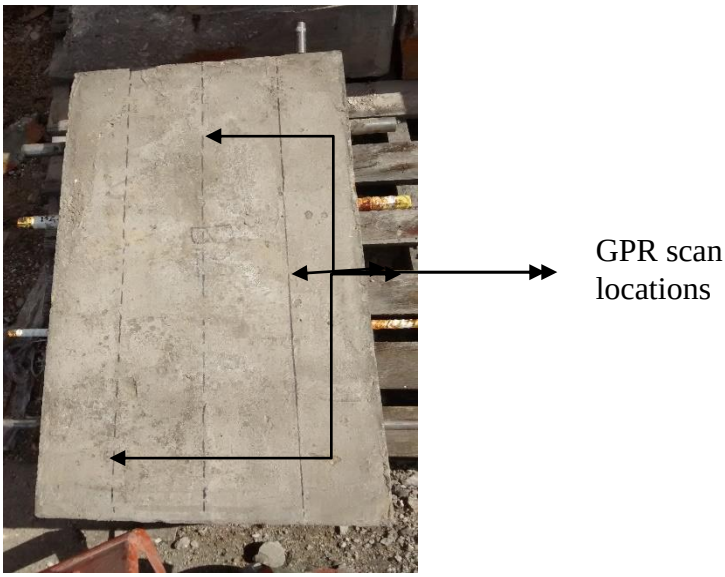

Figure 3-15: GPR scan locations

As mentioned previously, GPR scans were made at three different times:

1. After curing but before immersion into salt water
2. After salt water immersion but before passing current
3. At the end of the corrosion period

Before taking GPR measurements, it was made sure that the concrete surface was surface dry. This was done to avoid the effect of moisture content on GPR readings. Also, electronic devices (like mobile phones, circuit boards) were placed away while taking the readings. GPR wave forms at different cover depths are shown in Figure 3-16 and 3-17.

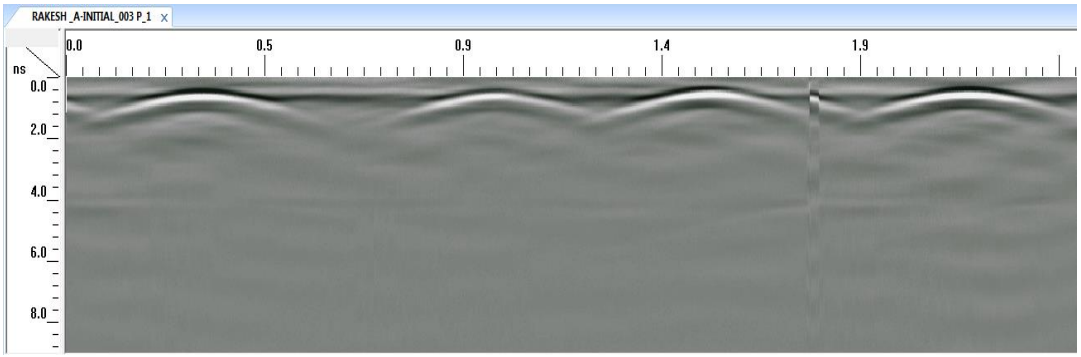

(a) GPR waveform before immersion

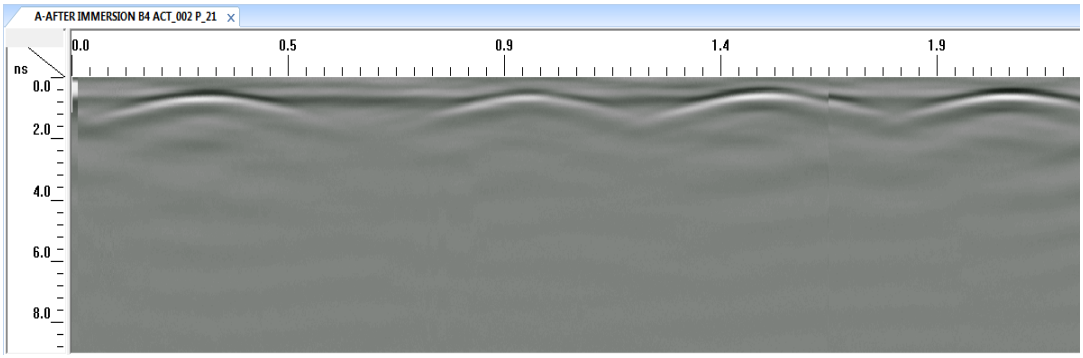

(b) GPR waveform after immersion

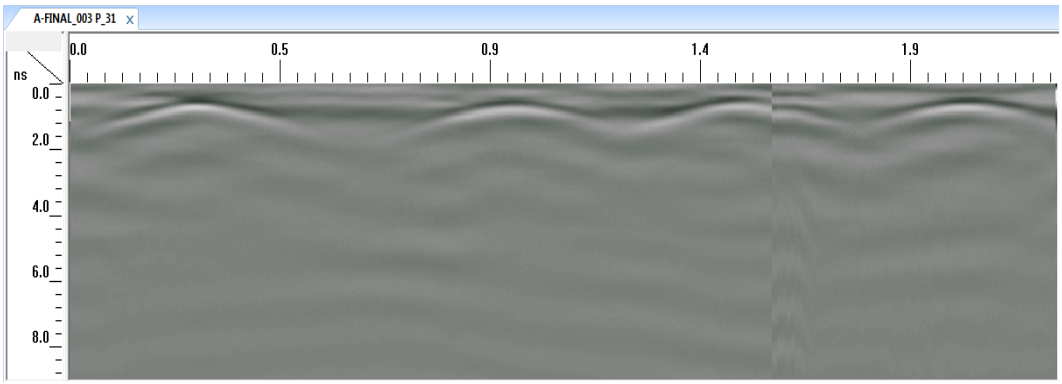

(c) GPR waveform at the end of corrosion period

Figure 3-16: GPR waveform from specimen A1 at different stages of corrosion

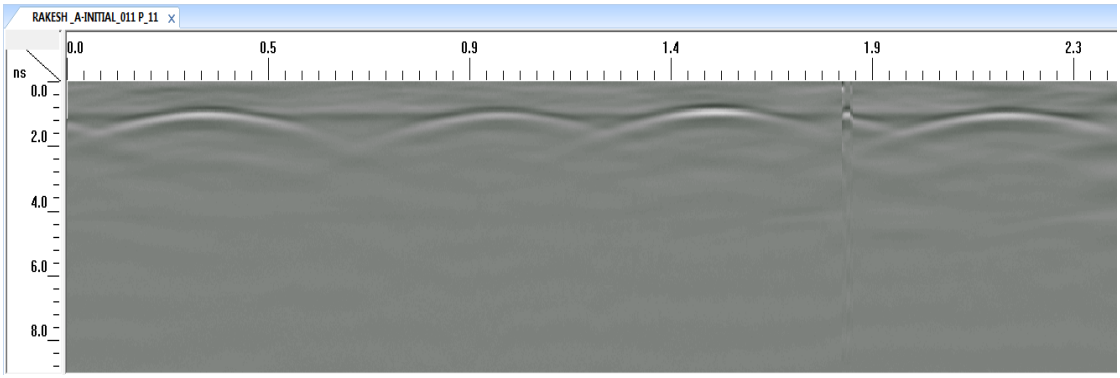

(a) GPR waveform before immersion

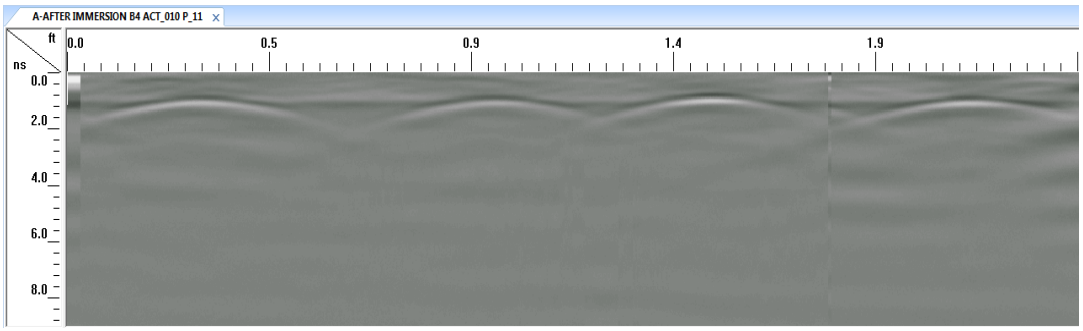

(b) GPR waveform after immersion

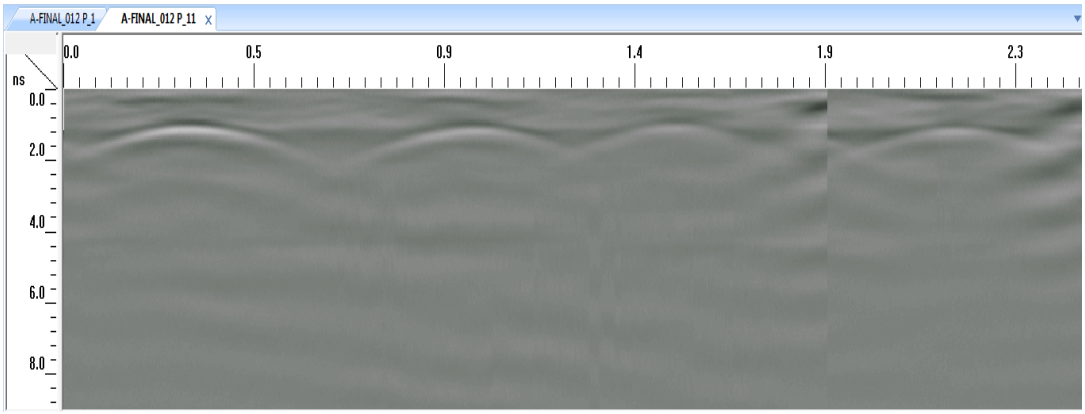

(c) GPR waveform at the end of corrosion period

Figure 3-17: GPR waveform from specimen A2 at different stages of corrosion

3.5 Rebar Mass Loss

After corrosion process, the samples were carefully broken with a hammer, and the rebars were taken out to determine the rebar mass loss (Figure 3-18)

Figure 3-18: Extraction of rebars from the specimens

ASTM G1 - 03(2011) - Standard practice for preparing, cleaning, and evaluating corrosion test specimens, was followed to determine the amount of rebar weight loss due to corrosion. Chemical cleaning procedure involved the preparation of a solution containing 0.265 gallon (1000 mL) hydrochloric acid (specific gravity 1.19), 0.044lb. (20 g) antimony trioxide and 0.11 lb. (50 g) stannous chloride vigorously stirred. The rebars were immersed in this solution at a temperature of 68 F (20 C) to 77 F (25 C) for about 1 to 25 minutes.

After the corrosion products were removed, the rebars were washed thoroughly with water and allowed to air dry. Once dried, their weights were taken and recorded and compared with their initial weights to determine the rebar mass loss due to corrosion.

From Figure 3-19, it is clear that the corrosion had occurred uniformly throughout the rebar length. Any pitting corrosion that had occurred at the rebar projections was not taken into consideration in the rebar mass loss determination.

(a) Rebars before cleaning

(b) Rebars after cleaning

Figure 3-19: Rebars before and after cleaning process

Chapter 4

Results and Discussions

In this research, an attempt was made to quantitatively relate different levels of corrosion in concrete rebars with the maximum amplitude of GPR waveform. Effort was also made to highlight the effect of corrosion on other parameters like two way travel time, dielectric constant, different rebar sizes and different concrete covers.

Change in amplitude and two way travel times at three different levels of corrosion were considered.

4.1 Effect of different phases of corrosion on amplitude

The maximum positive amplitude of GPR waveforms was found to change at different phases of corrosion. In the beginning, it was found to be maximum. During chloride contamination phase, seeping in of salt solution and accumulation of ions around the rebars resulted in two simultaneous effects. First, accumulation of ions decreased maximum positive amplitude of the reflected waveform. Second, absorption of GPR wave energy increased two way travel time. These ions further damaged the passive layer of rebar resulting in initiation of corrosion.

As the corrosion process continued, corrosion products dispersed within the concrete pores. As a result, travel time from the direct wave to anode bar was

reduced resulting in increased maximum positive amplitude. Stable ions in the anode were continuously consumed to produce corrosion products, which expanded, leading to the formation of micro-cracks within the concrete cover. Multiple interfaces (such as steel, corrosion product, concrete and cracks) in addition to outward movement of corrosion products generated wider radar footprints of radar waveforms during the course of corrosion (Figure 4-1).

Figure 4-1: Dispersion of corrosion products around rebar

Dispersion of corrosion products inside the concrete cover reduced the two way travel time and shortened the wavelength of rebar reflection resulting in greater maximum positive amplitude values at the end of corrosion period (Figure 4-2, 4-3).

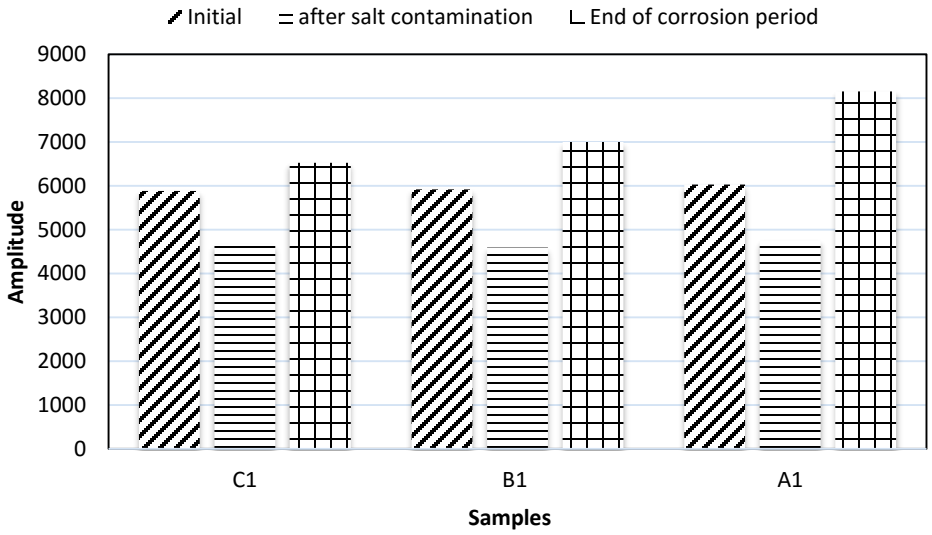

(a) # 4 (12.7 mm) rebar with 1" (25 mm) cover

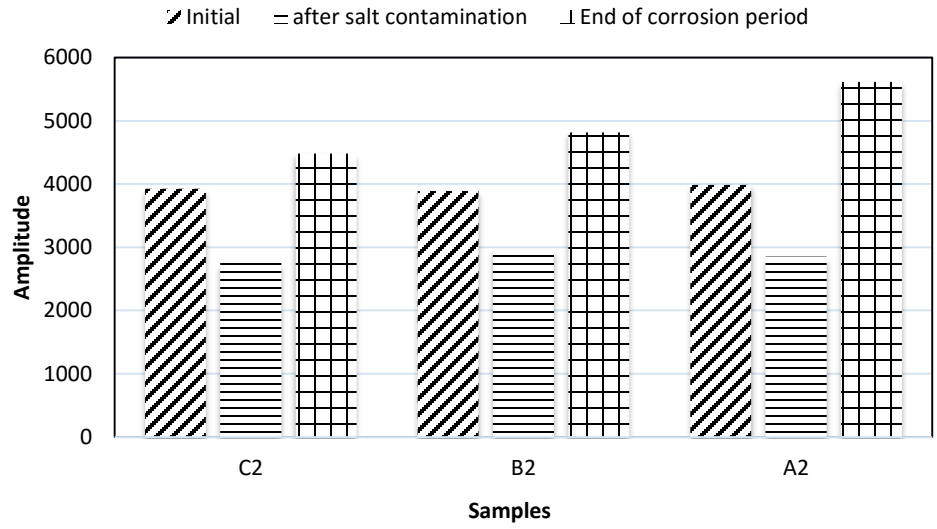

(b) # 4 (12.7 mm) rebar with 2" (50 mm) cover

Figure 4-2: Variation of GPR Amplitude for # 4 rebar

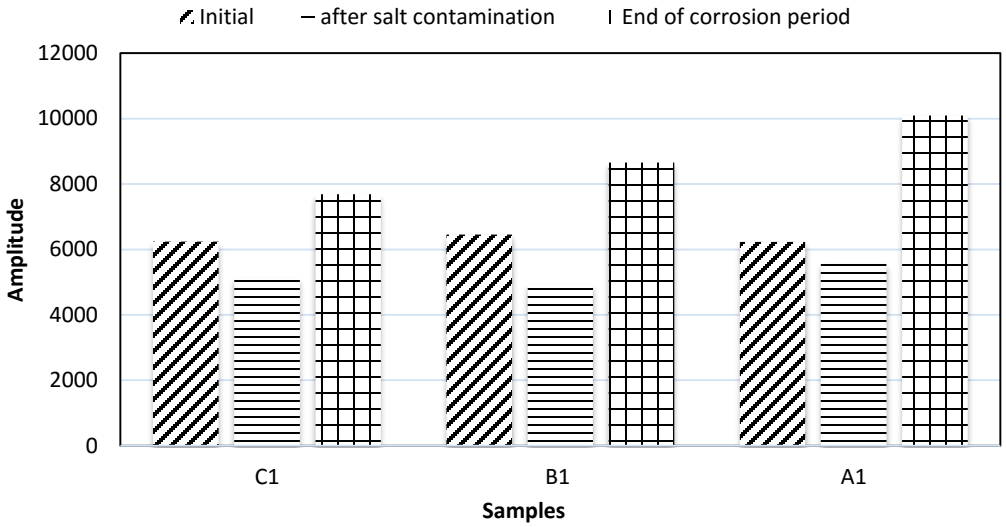

(a) # 7 (22.22 mm) rebar with 1” (50 mm) cover

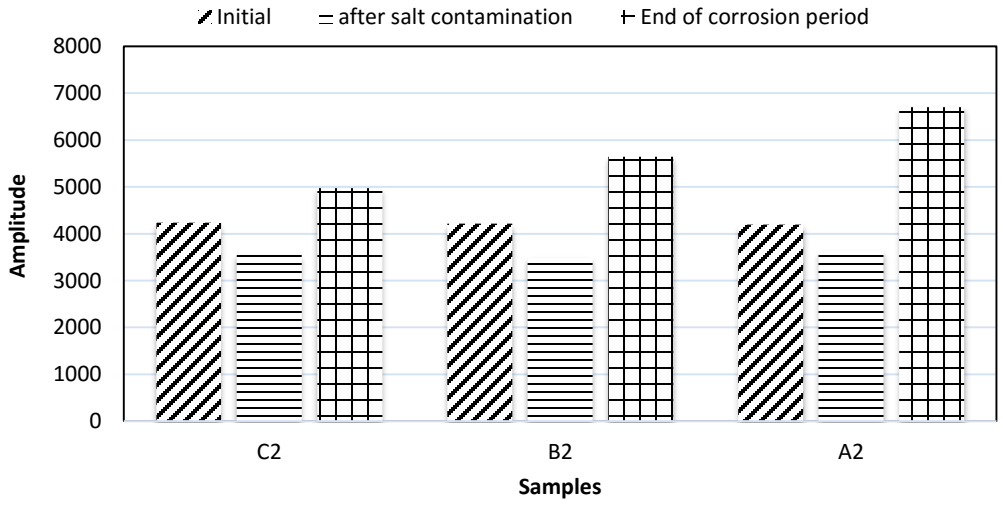

(b) # 7 (22.22 mm) rebar with 2” (50 mm) cover

Figure 4-3: Variation of GPR Amplitude for # 7 rebar

4.2 Effect of different rebar diameter on amplitude

The maximum positive amplitude of reflected GPR waveforms were plotted against corresponding diameters and concrete cover depth. Figure 4-4 shows the variation of maximum positive amplitude with increase in rebar diameter and concrete cover. It was observed that the amplitude value increased with increase in rebar diameter. It was because of the fact that the more rebar surface area was exposed to corrosive environment in case of # 7 (22.22 mm) rebar than # 4 (12.7 mm) rebar. Due to the formation of more corrosion products over #7 (22.22 mm) rebar, relatively higher decrease in dielectric constant of concrete cover was observed resulting in higher amplitude when compared with # 4 (12.7 mm) rebar.

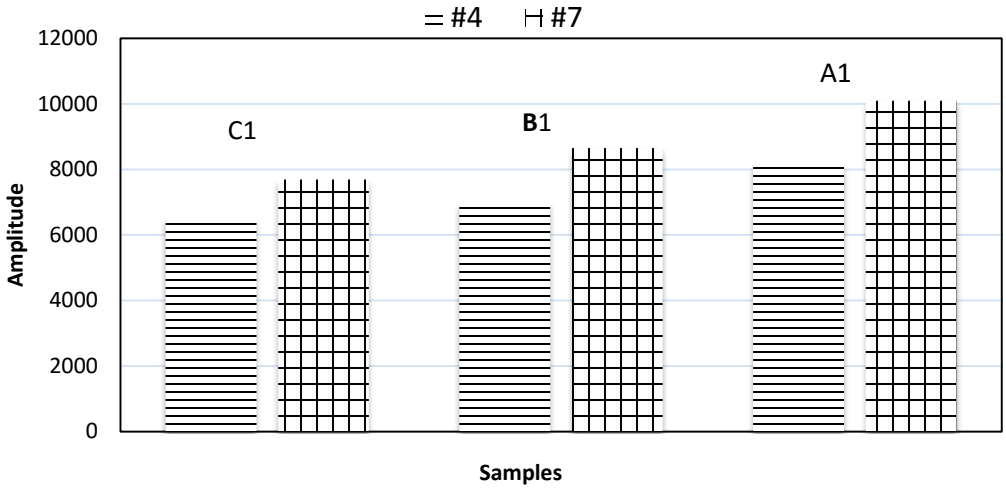

(a) 1” (25 mm) cover

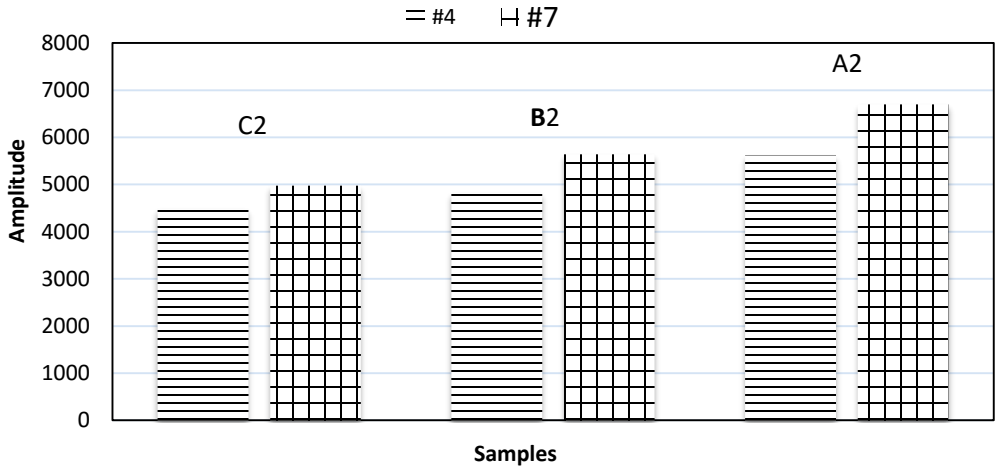

(b) 2” (50 mm) cover

Figure 4-4: Effect of Rebar Size on GPR amplitude

4.3 Effect of different concrete cover depth on amplitude

In order to study the effect of different concrete cover Figure 4-5 was plotted. Figures high light that the amplitude values are lesser for 2” (50mm) cover than that of 1” (25mm) cover. It is because of the reason that the radar waves had to travel longer distance at greater cover depths during which most of the radar energy is absorbed. Greater the depth more will be the loss of radar energy and less will be the amplitude of the reflected wave.

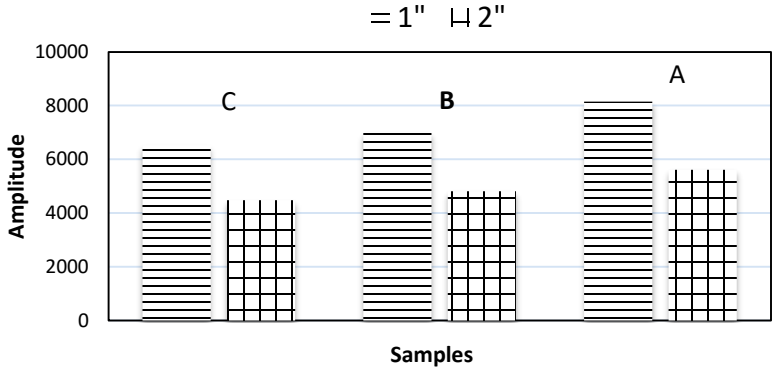

(a) #4 (12.7 mm) rebar

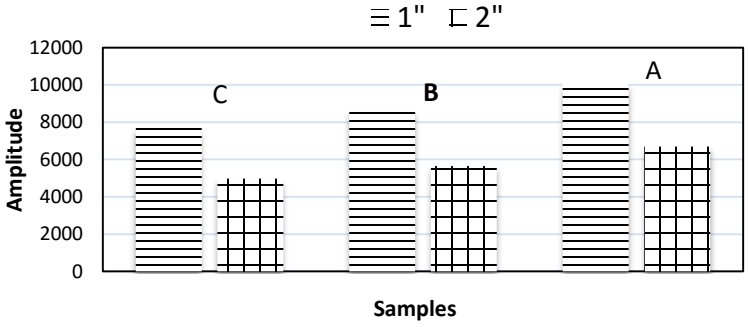

(b) #7 (22.22 mm) rebar

Figure 4-5: Variation of GPR amplitude with different concrete cover

4.4 Effect different phases of corrosion on TWTT

Two way travel time of reflected wave forms were plotted against different phases of corrosion for different rebar diameters at different cover depths with increase in corrosion levels as shown in figure 4-6 & 4-7. It can be observed that TWTT increases during salt water contamination phase and decreases to a value less than its original at the end of corrosion period.

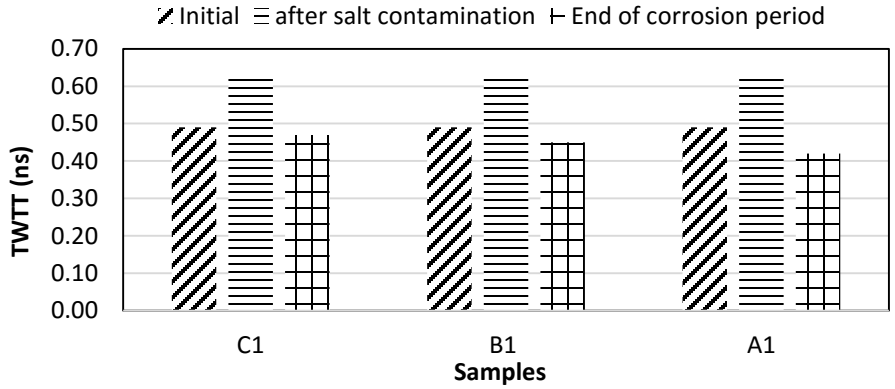

(a) # 4 (12.7 mm) rebar with 1" (25 mm) cover

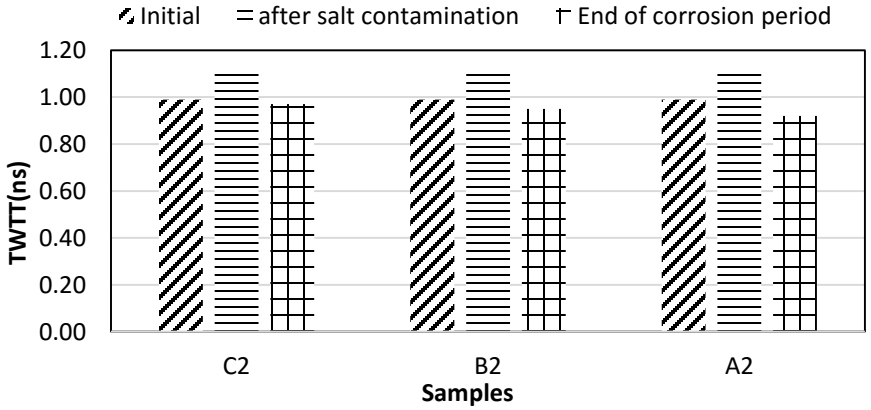

(b) # 4 (12.7 mm) rebar with 2" (50 mm) cover

Figure 4-6: Variation of TWTT at different phases of corrosion for # 4 rebar

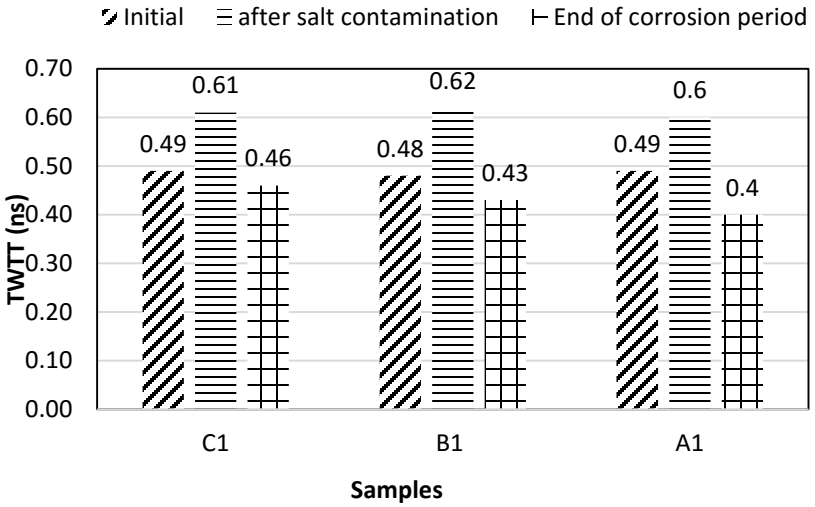

(c) # 7 (22.22 mm) rebar with 1" (25 mm) cover

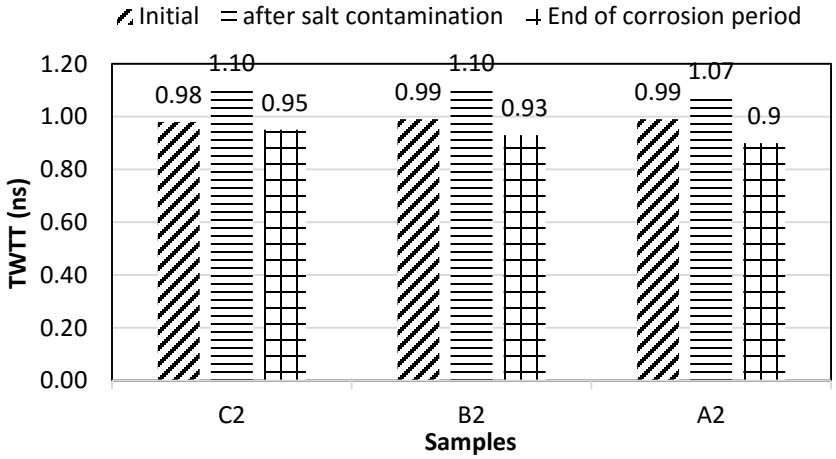

(d) # 7 (22.22 mm) rebar with 2" (50 mm) cover

Figure 4-7: Variation of TWTT at different phases of corrosion for # 7 rebar

Increase in TWTT is observed due to the increase in moisture content within the concrete pores as it was immersed in salt water during contamination

phase. And later restoration of original TWTT (decrease in its value), is observed due to the drying up of concrete cover and dispersion of corrosion products within that zone. This is also an indicative of the increase in dielectric property of concrete

4.5 Effect of different diameters at different concrete cover depth on TWTT

As discussed earlier, similar to amplitude TWTT also varies with different rebar diameters at different concrete cover (Table 4-1.4-2 & 4-3). Even though not much of difference exists between TWTT of different rebar diameters, there is significant difference in TWTT of rebars at different cover depths. This is attributed to the fact that waves have to travel double the distance in concrete of 2" (50 mm) cover than 1" (25 mm) cover. As a results, more the concrete cover more will be the TWTT.

Table 4-1: Variation of TWTT for C1 & C2

Rebar	Cover, in.(mm)	Time (days)	TWTT (ns)
#4 (12.7 mm)	1 (25)	1	0.49
		10	0.62
		20	0.47
	2 (50)	1	0.99
		10	1.11
		20	0.97
#7 (22.22 mm)	1 (25)	1	0.49
		10	0.61
		20	0.46
	2 (50)	1	0.98
		10	1.10
		20	0.95

Table 4-2: Variation of TWTT for B1 &B2

Rebar	Cover, in. (mm)	Time (days)	TWTT (ns)
#4 (12.7 mm)	1 (25)	1	0.49
		10	0.62
		30	0.45
	2 (50)	1	0.99
		10	1.10
		30	0.95
#7 (22.22 mm)	1 (25)	1	0.48
		10	0.62
		30	0.43
	2 (50)	1	0.99
		10	1.10
		30	0.93

Table 4-3: Variation of TWTT for A1 &A2

Rebar	Cover, in. (mm)	Time (days)	TWTT (ns)
#4 (12.7 mm)	1 (25)	1	0.49
		10	0.62
		40	0.42
	2 (50)	1	0.99
		10	1.10
		40	0.92
#7 (22.22 mm)	1 (25)	1	0.49
		10	0.60
		40	0.40
	2 (50)	1	0.99
		10	1.07
		40	0.90

4.6 Effect of different levels of corrosion on Dielectric constant of concrete cover

Dielectric constant is a parameter dependent on TWTT. Figure 4-8 & 4-9 shows the variation of dielectric constant of concrete cover at different levels of corrosion for different rebar diameter at different cover depths. It can be observed that the dielectric constant is decreasing with increase in corrosion levels.

As a matter of fact, with increase in corrosion levels more corrosion products are formed which tends to spread within the concrete pores in the weakest direction possible. Since concrete cover is relatively porous than other parts of concrete, corrosion products tend to spread within it. This in turn reduces TWTT of the reflected wave resulting in reduction in dielectric constant of the concrete cover as the corrosion process continues.

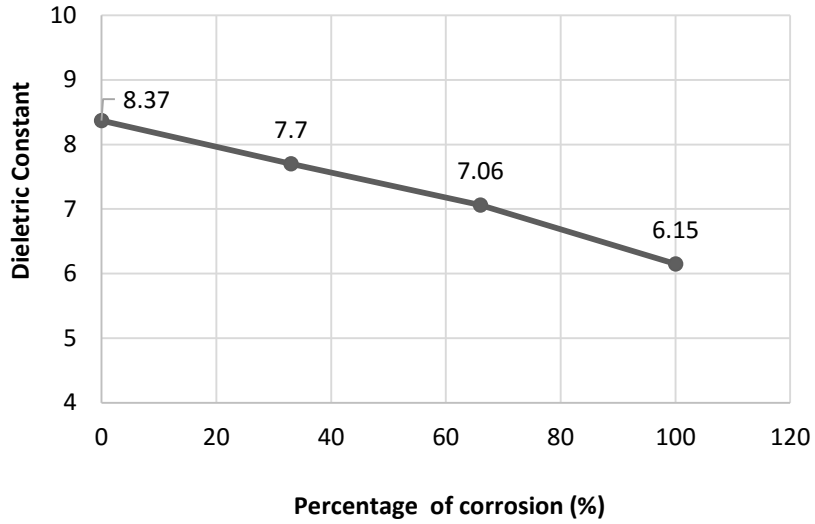

(a) # 4 (12.7 mm) rebar with 1” (25 mm) cover depth

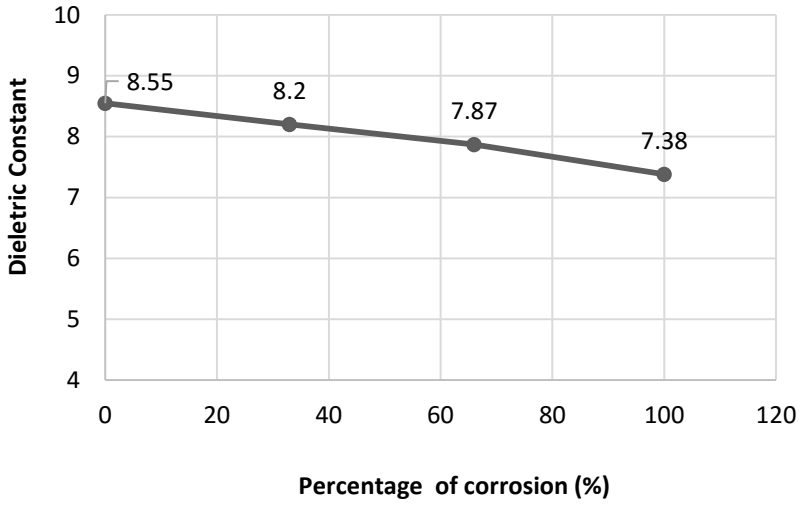

(b) #4 (12.7 mm) rebar with 2” (50 mm) cover depth

Figure 4-8: Variation of dielectric constant with different corrosion levels for # 4 rebar

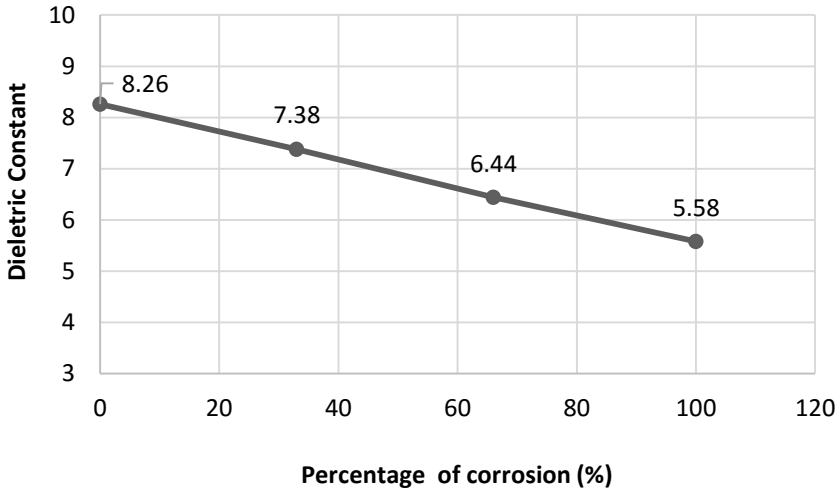

(a) #7 (22.22 mm) rebar with 1” (25 mm) cover

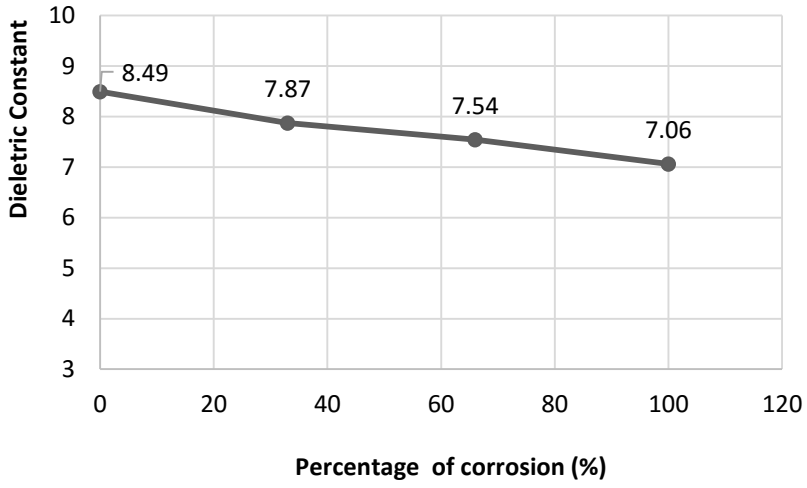

(b) #7 (22.22 mm) rebar with 2” (50 mm) cover

Figure 4-9: Variation of dielectric constant with different corrosion levels for # 7 rebar

4.7 Rebar mass loss at different corrosion levels

Loss in the rebar mass at the end of the corrosion period was calculated and tabulated in the Table 4-4 as shown. Since all the parameters that would affect accelerated corrosion was maintained constant from beginning till the end, percentage mass loss obtained approximately matched its corrosion levels.

Table 4-4: Mass loss of rebars subjected to different corrosion period

Specimen	Rebar specification	Wt. before corrosion, lb. (g)	Wt. after corrosion, lb. (g)	Wt. loss (lb.)	% Wt. loss
A1	#4 (12.7 mm) - 1” (25 mm) cover	1.14 (517.09)	1.018 (461.76)	0.122(55.33)	10.702
B1		1.14 (517.09)	1.067 (483.98)	0.073(33.11)	6.377
C1		1.12 (508.02)	1.083 (491.24)	0.037(16.78)	3.295
A2	#4 (12.7 mm) - 2” (50 mm) cover	1.12 (508.02)	1.029 (466.74)	0.091(41.27)	8.125
B2		1.12 (508.02)	1.058 (479.90)	0.062(28.12)	5.545
C2		1.12 (508.02)	1.092 (495.32)	0.028(12.70)	2.464
A1	#7 (22.22 mm) - 1” (25 mm) cover	3.50 (1587.57)	3.201(1451.95)	0.30(135.62)	8.543
B1		3.52 (1596.64)	3.315(1503.65)	0.205(92.98)	5.824
C1		3.48 (1578.50)	3.377(1531.78)	0.103(46.72)	2.960
A2	#7 (22.22 mm) - 2” (50 mm) cover	3.52 (1596.64)	3.302(1497.76)	0.218(98.88)	6.193
B2		3.52 (1596.64)	3.383(1534.51)	0.137(62.14)	3.892
C2		3.52 (1596.64)	3.471(1574.42)	0.049(22.22)	1.392

Percentage mass loss was found to be maximum for specimen subjected to longest corrosion period with least rebar diameter and least value of concrete cover depth. During rebar mass loss calculation length of rebar that was extended outside the concrete specimen for making electrical contacts is not taken into account.

4.7 Quantitative relationship between mass loss and amplitude

Figures 4-10 & 4-11 give the quantitative relationship between the rebar mass loss due to corrosion and the corresponding maximum positive amplitude. As discussed earlier, amplitude increases with increase in corrosion level due to the decrease in TWTT and change in dielectric property of concrete cover. These relations can be used in cases where dielectric constant of concrete for a particular level of corrosion matches with the ones mentioned in section 4.6.

Best fit line was drawn and the mathematical equation was suggested (Table 4-6) which can be used to approximate the amplitude values for a given level of corrosion in the absence of graphical data.

Before finalizing the best fit line, various trend lines were drawn for a given amplitude and mass loss relationship. Value of R^2 was derived from the graph which determines the accuracy of the best fit line. Based on the R^2 value, final best fit line was chosen for which R^2 value was close to 1. Table 4-5 provides R^2 value for various trend lines for # 4 rebar with 1" cover.

Table 4-5: Trend lines and corresponding R^2 values for #4 (12.5) rebar with 1” (25mm) cover

Trend line	R^2
Linear	0.9835
Exponential	0.9926
Polynomial	0.9979

From Table 4-5, it can be seen that the for a trend line of type “polynomial”, R^2 value is closest to 1. Hence, polynomial trend line was chosen as the best fit line to draw the GPR amplitude and percentage mass loss relationship.

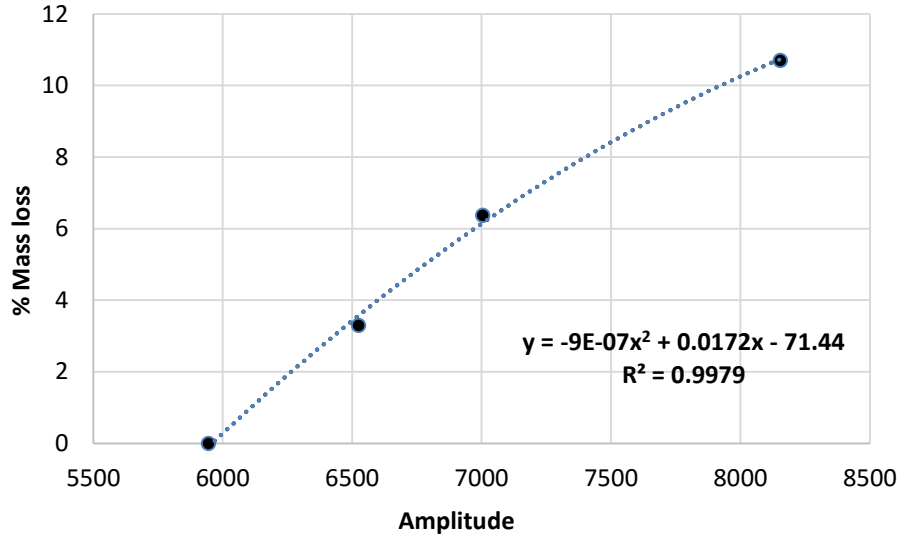

(a) #4 (12.7 mm) rebar with 1” (25 mm) cover

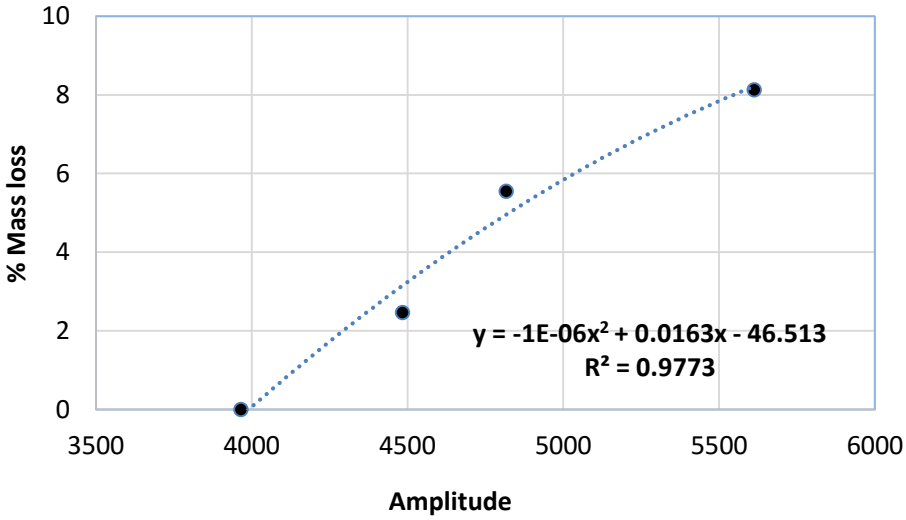

(b) #4 (12.7 mm) rebar with 2” (50 mm) cover

Figure 4-10: Quantitative relationship between GPR amplitude and percentage mass loss for # 4 rebar

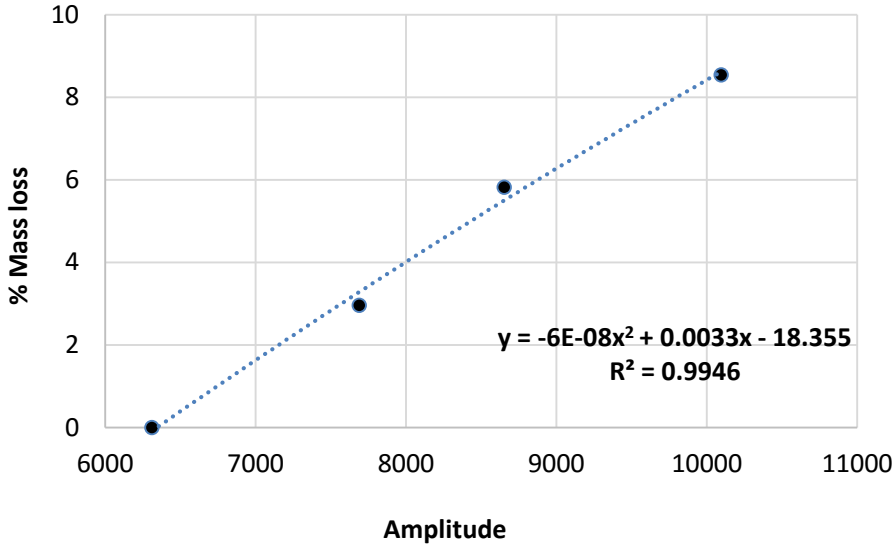

(a) #7 (22.22 mm) rebar with 1” (25 mm) cover

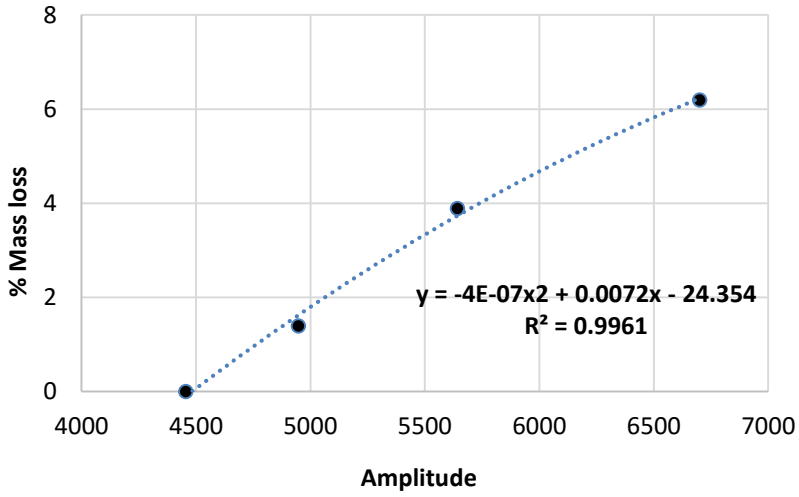

(b) #7 (22.22 mm) rebar with 2” (50 mm) cover

Figure 4-11: Quantitative relationship between GPR amplitude and percentage mass loss for # 7 rebar

Table 4-6: Equation for estimation of corrosion from GPR amplitudes

Rebar	Cover, in (mm)	Equation
# 4	1 (25)	$y = -9E\text{-}07x^2 + 0.0172x - 71.44$
	2 (50)	$y = -1E\text{-}06x^2 + 0.0163x - 46.513$
# 7	1 (25)	$y = -6E\text{-}08x^2 + 0.0033x - 18.355$
	2 (50)	$y = -4E\text{-}07x^2 + 0.0072x - 24.354$

Where,

x = GPR amplitude

y = % mass loss

4.8 Comprehensive prediction model

In order to obtain the comprehensive prediction model of corrosion that includes variation of both rebar diameter and concrete cover, GPR amplitudes of each rebar with their corresponding concrete cover was normalized with respect to their initial GPR reading obtained when there was no corrosion in the rebars (Figure 12). This model predicts the amount of corrosion quantitatively only if the GPR amplitude with respect to which the other amplitudes are normalized corresponds to zeroth corrosion level.

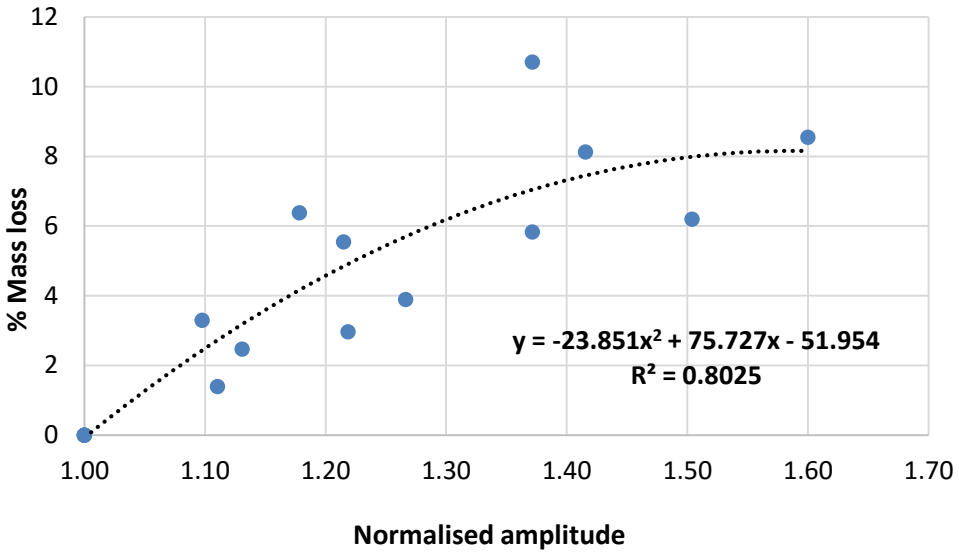

Figure 12: Comprehensive prediction model

In the absence of initial GPR reading, normalization can be done with respect to the GPR amplitude collected from the region free from corrosion (within the same structure) followed by visual inspection by exposing a part of the rebar.

Since the selection of normalization amplitude is purely dependent on the experience of the GPR user, this model can generally be used to predict rebar mass loss qualitatively.

Thus in the absence of normalized amplitude, it is recommended to use relationships obtained in section 4.8 to predict amount of rebar mass loss quantitatively.

Chapter 5

Experimental Verification

5.1 Bridge deck sample

A part of old bridge deck situated on I30 Dallas was chosen to verify the experimental results obtained in the laboratory conditions (Figure 5-1).

Figure 5-1: Specimen obtained from I30 bridge deck

5.2 GPR data collection

Due to the unevenness of the top surface a thin sheet of plywood of negligible thickness was kept on its tops surface and the data was collected. GPR waveform of the naturally corroded # 4 (12.7 mm) rebar is as shown in figure 5-2.

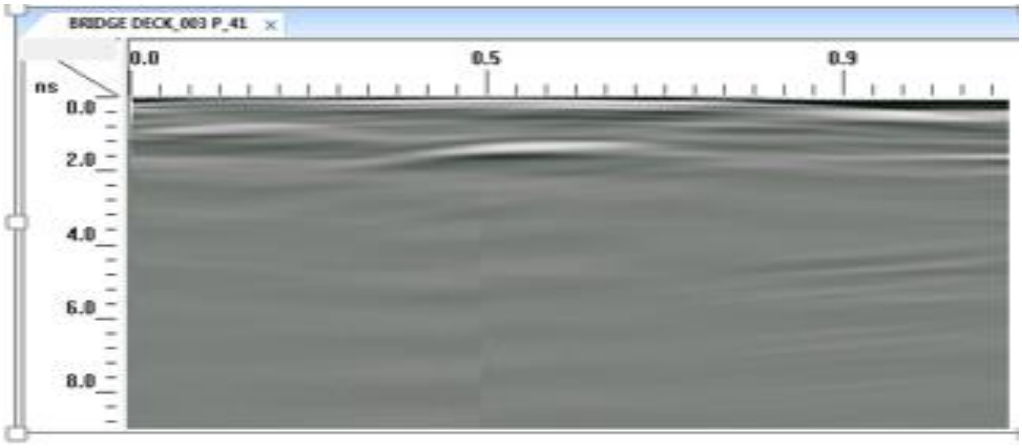

Figure 5-2: GPR waveform of #4 (12.7 mm) rebar

Once the GPR data was collected, it was taken to RADAN and further processed to obtain the parameters such as amplitude and TWTT.

Table 5-1: GPR results from the bridge deck sample

Rebar	Cover, inches (mm)	Amplitude	TWTT (ns)	Dielectric constant
#4 (12.7 mm)	2 (50)	5512	0.9	7.06
	2 (50)	5643	0.9	7.06
	2 (50)	6120	0.89	6.90
	Average	5758	0.90	7.01

5.3 Rebar mass loss

5.3.1 Rebar cleaning

Once the GPR results were obtained, the corroded rebar was taken out and cleaned as per the procedure mentioned in section 3.6 and weighed to obtain the percentage rebar mass loss due to natural corrosion.

Figure 5-3: Rebar location

From Figure 5-3 it was clear that corrosion of rebar had occurred only at the top and the reflected waveform of the GPR taken corresponds to the corroded part of the rebar.

(a) Rebar before cleaning

(b) Rebar after cleaning

Figure 5-4: Corroded rebar during cleaning process.

5.3.2 Rebar mass loss determination

Rebar size: #4 (12.7 mm)

Concrete cover: 2” (50 mm)

Length of rebar = 8” (203 mm)

Weight of plf of # 4 (12.7 mm) rebar = 0.668 lb. /ft. (0.994 kg/m)

Weight of rebar /11” (280 mm) length = (0.668/12) x 8 = 0.4453 lb. (202 g)

Weight of rebar after mass loss = 0.4173 lb. (189.284 g)

Mass loss of rebar = 0.4453 – 0.4173 = 0.028 lb. (12.7g)

% mass loss of rebar = (0.028 x 100) / 0.4453 = 6.287 %

This value was compared with the results obtained from experimental results in laboratory.

From figure 4.7 (b),

Corresponding to 5758 amplitude percentage rebar mass expected = 8.125%

Actual percentage mass loss in bridge deck = 6.288 %

% Error: {(8.125 – 6.288)/8.125} x 100 = 22.60 %

5.4 Results and Discussions

After comparing the results of accelerated corrosion achieved in laboratory conditions and natural corrosion of rebar in bridge deck, an error of 22.6% in the prediction of rebar mass loss was observed. Various reasons that can be attributed to this error are as follows:

- Dissimilarity in the nature of corrosion

  Under laboratory conditions, rebar had corroded uniformly throughout the length and around the circumference of the rebar, wherein in case of rebar obtained from the bridge deck corrosion had happened only on its top surface.

  Since GPR waves cannot penetrate through the rebar diameter, the amplitude value corresponds to the corrosion that has occurred only on the top surface of the rebar and any corrosion that occurs at the bottom surface of the rebar goes undetected. This supports the fact that the laboratory results predicts higher amount of rebar mass loss for a given value of maximum positive GPR amplitude.

- Corrosion period and rate

  According to Maaddawy et.al 2003, initiation of accelerated corrosion of rebar in concrete leads to higher concentration of corrosion products around the rebars and diffusion of these products in to the

concrete pores will be to a little extent. As a result variation of dielectric properties of concrete around the rebar will be minimal.

On the other hand, in case of natural corrosion, corrosion products diffuse in to the surrounding concrete pores to a greater extent, leading to significant variation in dielectric property of the concrete. Since GPR amplitude is maximum for a concrete of lower dielectric constant, higher GPR amplitude is obtained in case of bridge deck for a given amount of corrosion.

Also other factors that might have lead this error might be age, strength and nature of concrete ingredients like admixtures, chlorides and moisture content (Pokkuluri, 1998).

Chapter 6

Conclusions

6.1 Research Conclusions

Based on experimental test results of this research work following conclusion can be drawn:

- Due to the formation of more corrosion products over #7 (22.22 mm) rebar, higher decrease in dielectric constant of concrete cover was observed resulting in relatively higher amplitude than that obtained in case of # 4 (12.7 mm) rebar. This concludes that the increase in rebar diameter increases amplitude of GPR waveform.
- GPR amplitude was more in case of 1” (25 mm) cover than 2” (50 mm) cover. It is because of the reason that the radar waves had to travel longer distance at greater cover depths during which most of the radar energy is absorbed. Greater the depth more will be the loss of radar energy and less will be the amplitude of the reflected wave.
- Even though not much of difference exists between TWTT of different rebar diameters, there is significant difference in TWTT of rebars at different cover depths. This is attributed to the fact that waves have to travel double the distance in concrete of 2” (50 mm)

cover than 1” (25 mm) cover. As a results, more the concrete cover more will be the TWTT.

- Amount of mass loss due to corrosion can be quantitatively related to maximum positive amplitude of reflected wave.
- Quantitative relation drawn between the amplitude and the mass loss of rebar in concrete due to corrosion can be used in cases where the dielectric constant of concrete cover, TWTT of radar wave, frequency of antenna used and surface conditions of concrete specimen matches with the one employed in this study.
- Similar to amplitude, variation in TWTT and dielectric constant corresponding to different phases of corrosion, different rebar diameter at different concrete can be established.
- Variation in GPR parameters with corrosion phases and levels observed in this study are in good agreement with the previous studies.
- Comprehensive model is being predicted which takes into account of variation in rebar diameter and concrete cover.
- Verification of accelerated corrosion with natural corrosion of rebar in a bridge deck yielded 22.2 % error, which is acceptable due to complexity involved in corrosion mechanism.

6.2 Recommendations and Future work

- This study uses GPR antenna of frequency 2.6 GHz to quantitatively relate amplitude with amount of rebar mass loss in concrete. It is suggested to use antenna of other frequencies and from other manufacturers to see the variation in amplitude values at different corrosion levels.
- In this study concrete of strength 4.9 ksi is used. Variation in GPR parameters with different concrete strengths and also concrete of different dielectric constants should also be investigated.
- This study uses rebars of diameter #4 (12.7 mm) and #7 (22.22 mm). As discussed earlier, that rebar size effects the GPR parameters like amplitude and TWTT, it is recommended to establish quantitative relationship between amplitude and rebar mass loss for other rebar diameters.
- More comparative study needs to be done on the usage of the relationship (amplitude and % rebar mass loss) obtained in this study in the natural scenarios in order to evaluate the extent of its application.

References

A. K. Azad, S. Ahmad, and S. A. Azher, "Residual Strength of Corrosion-Damaged Reinforced Concrete Members", *ACI Materials Journal*, 104(1) (2007), pp. 303–310.

A. A. Almusallam, A. S. Al-Gahtani, A. R. Aziz, and Rasheeduzzafar, "Effect of Reinforcement Corrosion on Bond Strength", Construction and Building Materials, 10(2)(1996), pp. 123–129.

ASTM G1-03(2011), Standard Practice for Preparing, Cleaning, and Evaluating Corrosion Test Specimens, ASTM International, West Conshohocken, PA, 2011

B. H. A. Al-Gohi, "Time-Dependent Modeling of Loss of Flexural Strength of Corroding RC Beams", *MS thesis* submitted to King Fahd University of Petroleum & Minerals, Saudi Arabia, May 2008.

Broomfield, John P. *Corrosion of steel in concrete: understanding, investigation and repair*. CRC Press, 2002.

C. C. Yang, "The Relationship between Charge Passed and the Chloride Concentrations in Anode and Cathode Cells Using the Accelerated Chloride Migration Test", *Materials and Structures*, 36(2003), pp. 678–684.

Chang, Che Way, Chen Hua Lin, and Hung Sheng Lien. "Measurement radius of reinforcing steel bar in concrete using digital image GPR." Construction and Building Materials 23.2 (2009): 1057-1063.

Daniels, David J. *Ground penetrating radar*. Vol. 1. Iet, 2004.

F. P. Ijsseling, "Application of Electrochemical Methods of Corrosion Rate Determination to System Involving Corrosion Product Layers", *British Corrosion Journal*, 21(2)(1986), pp. 95–101.

Garboczi, E. J., Stutzman, P. E., Wang, S., Martys, N. S., Hassan, A., Duthinh, D., & Stiles, M. D (2010). Corrosion Detection in Concrete Rebars Using a Spectroscopic Technique.

Hong, S., Lai, W. W. L., Wilsch, G., Helmerich, R., Helmerich, R., Günther, T., & Wiggenhauser, H. (2014). Periodic mapping of reinforcement corrosion in intrusive chloride contaminated concrete with GPR. Construction and Building Materials, 66, 671-684

Hubbard, Susan S., et al. "Experimental detection of reinforcing bar corrosion using nondestructive geophysical techniques." ACI Materials Journal 100.6 (2003).

J. Rodriguez, L. M. Ortega, and J. Casal, “Load Carrying Capacity of Concrete Structures With Corroded Reinforcement”, Construction and Building Materials, 11 (4)(1997), pp. 239–248.

J. Wei-liang and Z. Yu-xi, “Effect of Corrosion on Bond Behavior and Bending Strength of Reinforced Concrete Beams”, Journal of Zhejiang University (SCIENCE), 2(3)(2001), pp. 298–308.

K. Stanish, R. D. Hooton, and S. J. Pantazopoulou, “Corrosion Effects on Bond Strength in Reinforced Concrete”,ACI Structural Journal, 96(6)(1999), pp. 915–921.

L. Amleh and S. Mirza, “Corrosion Influence on Bond Between Steel and Concrete”, ACI Structural Journal, 96(3)(1999), pp. 415–423.

Mansfeld, Florian. "Area relationships in galvanic corrosion." Corrosion 27.10 (1971): 436-442.

Oldfield, John W. "Electrochemical theory of galvanic corrosion." *Galvanic Corrosion* (1988): 5-22.

P. S. Mangat and M. S. Elgarf, “Flexural Strength of Concrete Beams With Corroding Reinforcement”, ACI Structural Journal, 96(1)(1999), pp. 149–158.

R. Huang and C. C. Yang, “Condition Assessment of Reinforced Concrete Beams Relative to Reinforcement Corrosion”, Cement and Concrete Composites, 19(1997), pp. 131–137.

S. A. Austin, R. Lyons, and M. J. Ing, “Electrochemical Behavior of Steel-Reinforced Concrete During Accelerated Corrosion Testing”, *Corrosion*, 60(2)(2004), pp. 203–212.

S. A. Azher, “A Prediction Model for the Residual Flexural Strength of Corroded Reinforced Concrete Beams”, *MS thesis* submitted to King Fahd University of Petroleum & Minerals, Saudi Arabia, January 2005.

S. Ahmad, B. Bhattacharjee, and R. Wason, “Experimental Service Life Prediction of Rebar-Corroded Reinforced Concrete Structure”, ACI Materials Journal, 94(4)(1997), pp. 311–316.

S. Care and A. Raharinaivo, “Influence of Impressed Current on the Initiation of Damage in Reinforced Mortar due to Corrosion of Embedded Steel”, *Cement and Concrete Research*, 37(2007), pp. 1598–1612.

S. F. Ahmed, M. Maalej, P. Paramasivam, and H. Mihashi, “Assesment of Corrosion-Induced Damage and its Effect on the Structural Behavior of RC Beams Containing Supplementary Cementitious Materials”, *Progress in Structural Engineering and Materials*, 8(2)(2006), pp. 69–77.

S. Mangat and M. S. Elgarf, “Bond Characteristics of Corroding Reinforcement in Concrete Beams”, Materials and Structures, 32(1999), pp. 89–97.

Shaw, M. R., et al. "Assessing bar size of steel reinforcement in concrete using ground penetrating radar and neural networks." *Insight-Non-Destructive Testing and Condition Monitoring* 45.12 (2003): 813-816.

Shaw, M. R., et al. "Location of steel reinforcement in concrete using ground penetrating radar and neural networks." NDT & E International 38.3 (2005): 203-212.

Stratton, Julius Adams. *Electromagnetic theory*. John Wiley & Sons, 2007.

T. A. El Maaddawy and K. A. Soudki, “Effectiveness of Impressed Current Technique to Simulate Corrosion of Steel Reinforcement in Concrete”, *ASCE Journal of Materials in Civil Engineering*, 15(1)(2003), pp. 41–47.

T. H. Ha, S. Muralidharan, J. H. Bae, Y. C. Ha, H. G. Lee, K. W. Park, and D. K. Kim, “Accelerated Short-Term Techniques to Evaluate the Corrosion Performance of Steel in Fly Ash Blended Concrete”, *Building and Environment*, 42(2007), pp. 78–85.

Utsi, Vincent, and Erika Utsi. "Measurement of reinforcement bar depths and diameters in concrete." Ground Penetrating Radar, 2004. GPR 2004. Proceedings of the Tenth International Conference on. IEEE, 2004.

W. H. Hartt and R. P. Brown, “Laboratory Method for Corrosion Testing of Reinforced Concrete Using Impressed Current”, *Proceedings of Corros/’79 published by NACE,* March 12-16 (1979), pp. 133.1–133.7.

Y. Auyeung, P. Balaguru, and L. Chung, “Bond Behavior of CorrodedReinforcementBars”, ACI Materials Journal, 97(2)(2000), pp. 214–220.

Y. Tachibana, K. I. Maeda, Y. Kajikawa, and M. Kawamura, “Mechanical Behavior of RC Beams Damaged by Corrosion of Reinforcement”, Third International Symposium on Corrosion of Reinforcement in Concrete Construction, Wishaw, UK (1990), pp. 178–187.

Y. Yuan, Y. Ji, and S. P. Shah, “Comparison of Two Accelerated Corrosion Techniques for Concrete Structures”, *ACI Structural Journal*, 104(3)(2007), pp. 344–347

Biography

Rakesh Krishnarajapete Raju earned his Bachelors of Science degree in Civil Engineering at S.J.C.E. Mysore College in June 2014. During his study, he worked as an intern at Bluejay Enterprises Pvt. Ltd. and Prestige Estate Projects Ltd. Bangalore, India, wherein he gained handful of technical design/ planning aspects and management experience in the field. These strengths, with various technical and professional skills, motivated him to pursue Structural Engineering at University of Texas at Arlington.

His research interests are Non-destructive testing and evaluation, pre-stressed concrete, design of reinforced concrete structures and Evaluation of Earthquake resistant structures.